Formations and Applications of High-Performance Phase-Conjugate Mirrors in Cu-doped(k[0.5]Na[0.5])[0.2](Sr[0.61]Ba[0.39])[0.9]Nb[2]O[6]Photorefractive Crystals

THESIS

FORMATIONS AND APPLICATIONS OF HIGH-PERFORMANCE PHASE-CONJUGATE MIRRORS IN Cu-DOPED $(K_{0.5}Na_{0.5})_{0.2}(Sr_{0.61}Ba_{0.39})_{0.9}Nb_2O_6$ PHOTOREFRACTIVE CRYSTALS

Yujin ZHENG

Graduate School of Electronic Science and Technology
Shizuoka University

July 1997

Abstract

Optical phase-conjugate mirrors using photorefractive crystals are, by far, the most efficient devices for the generation of phase conjugate waves. In the present thesis the stable self-pumped phase-conjugate mirror (SPPCM), the high-performance double phase-conjugate mirrors (DPCMs) and the applications of the phase-conjugate mirrors (PCMs) are studied in photorefractive Cu-doped $(K_{0.5}Na_{0.5})_{0.2}(Sr_{0.61}Ba_{0.39})_{0.9}Nb_2O_6$ (Cu:KNSBN) crystals.

At first the origin and elimination of dynamic instability are further studied in a Cu:KNSBN SPPCM. The theory and experiment show that the self-generated fanning effect can be decreased with a partially extraordinary-polarized input light. The dynamic instability can be eliminated by restraining the self-generated fanning.

The second subject concerns how to form a high-performance DPCM in Cu:KNSBN crystals. A high-performance Cu:KNSBN modified-bridge DPCM with low light loss and strong coupled strength is formed. In another aspect, for the crystals with different absorption coefficients, the optimum incident geometries of the bridge DPCMs are discussed.

Next, a new type of multiple PCM consisting of a SPPCM and a DPCM is proposed in a Cu:KNSBN crystal. The performance of the multiple PCM is investigated. The real-time orthoscopic three-dimensional image projection using the multiple PCM is achieved by performing two phase-conjugate operations on the incident image.

Finally, an all-optical switching dynamic interconnection is demonstrated using the arrangement of the multiple DPCMs in a Cu:KNSBN crystal. An all-optical routing switching dynamic interconnection is also achieved, in which the routing dynamic interconnection is switched by inputting different control beams.

Contents

Chapter 1 Introduction 1

1.1 Optical Phase Conjugation and its Background 1

1.2 Outline of This Thesis 9

References 11

Chapter 2 Origin and Elimination of Dynamic Instability in a Self-Pumped Phase-Conjugate Mirror (SPPCM) 14

2.1 Introduction 14

2.2 Fanning Effect in Photorefractive Crystal 16

2.3 Experimental Certification on the Origin of Dynamic Instability in a Cu:KNSBN SPPCM 22

2.4 Theoretical Analysis and Experimental Study on the Elimination of Dynamic Instability in a SPPCM 27

2.5 Summary 34

References 35

Chapter 3 High-Performance Double Phase-Conjugate Mirror (DPCM) in Cu:KNSBN Crystal 37

3.1 Introduction 37

3.2 Four-Wave Mixing in a DPCM 38

3.3 Formation of the High-Performance DPCM with the Modified-Bridge Geometry 46

3.4 Summary 54

References 55

Chapter 4 High-Efficiency Bridge Double Phase-Conjugate Mirrors (DPCMs) in Cu:KNSBN Crystals 57

4.1 Introduction 57

4.2 Formation of the High-Efficiency Bridge DPCMs in Cu:KNSBN Crystals with Different Absorption Coefficients 58

4.3 Observation and Discussion of the Optimum Incident Geometries of DPCMs 61

4.4 Summary 67

References 68

Chapter 5 Multiple Phase-Conjugate Mirror (PCM) and Orthoscopic Projection of a Three-Dimensional (3D) Object in a Cu:KNSBN Crystal 69

5.1 Introduction 69

5.2 Two Phase-Conjugate Operations on an Input Light Wave 70

5.3 Formation of the Multiple PCM in a Cu:KNSBN Crystal 71

5.4 Performance of the Multiple PCM 74

5.5 Spatial Fidelity of the Multiple PCM and Real-Time Orthoscopic 3D Image Projection 77

5.6 Summary 82

References 83

Chapter 6 All-Optical Routing Switching Dynamic Interconnection with Multiple DPCMs 84

6.1 Introduction 84

6.2 All-Optical Switching Dynamic Interconnection

in a Cu:KNSBN Crystal 86

6.3 All-Optical Routing Switching Dynamic Interconnection 92

6.4 Summary 96

References 98

Chapter 7 Conclusion 99

7.1 Summary 99

7.2 Suggestions 101

Acknowledgements 103

List of Publications by the Author 104

Chapter 1

Introduction

1.1 Optical Phase Conjugation and its Background

Optical phase conjugation is a technique for reversing both the direction of propagation and the overall phase factor of an incoming light wave.[1-4] The process can be regarded as a unique kind of "mirror" with very unusual image-transformation properties. A beam reflected by a phase-conjugate mirror retraces its original path. This retroreflecting property of phase-conjugate waves is very useful in optical information processing, optical communication, optical interferometer, optical computing and adaptive optical interconnection,[5-17] and so on. In this chapter, we describe what is phase conjugation and its properties.

Figure 1.1 illustrates the remarkable difference between phase-conjugate reflection and conventional mirror reflection. A conventional plane mirror [Fig. 1.1(a)] changes the sign of the wave vector $\boldsymbol{k}$ component normal to the mirror surface while leaving the tangential component unchanged. An inputting light beam can thus be redirected arbitrarily by suitable tilting the mirror. On the other hand, the phase-conjugate mirror [Fig. 1.1(b)] causes an inversion of the vector quantity $\boldsymbol{k}$,

(a) Conventional Mirror

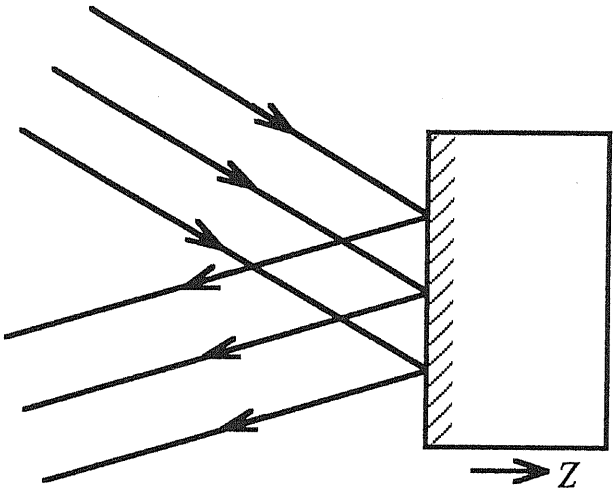

$$k_{in} = k_x\hat{x} + k_y\hat{y} + k_z\hat{z} \qquad k_{out} = k_x\hat{x} + k_y\hat{y} - k_z\hat{z}$$

(b) Phase-Conjugate Mirror

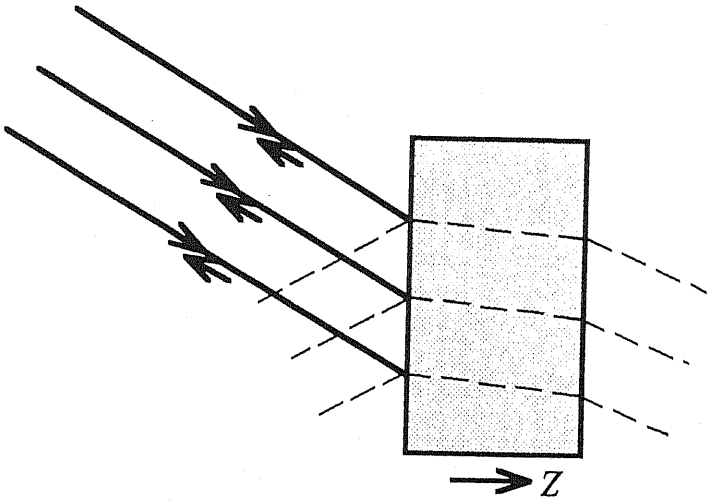

$$k_{out} = -k_{in}$$

Fig. 1.1. Comparison of a conventional mirror reflection and a phase-conjugate reflection. (a) Reflection of the plane mirror. (b) Reflection of phase-conjugate mirror. The mirror reflection reverses the k-vector component normal to its surface, whereas the phase-conjugate mirror reveres the vector quantity k.

so that the incident beam exactly returns upon itself and is independent of the orientation of the phase-conjugate mirror.

Now, we consider the propagation of an electromagnetic wave along the z-axis. Using analytic representation, the electric field can be written

$$\boldsymbol{E} = A(\boldsymbol{r})\exp\{i[\omega t - kz - \phi(\boldsymbol{r})]\}, \tag{1.1}$$

here ω is the frequency, and k is the wave number. The amplitude A and the phase ϕ are real functions of position (x, y, z). For any electromagnetic wave given by Eq. (1.1), its phase conjugate wave is given by

$$\boldsymbol{E}_c = A(\boldsymbol{r})\exp\{i[\omega t + kz + \phi(\boldsymbol{r})]\}. \tag{1.2}$$

$\boldsymbol{E}_c$ and $\boldsymbol{E}$ form a conjugate pair. We can see that these two waves have exactly the same wave fronts at any point in space. However, the motion of their wave fronts is in opposite directions. If we reverse the sign of the time variable in $\boldsymbol{E}$, we obtain $\boldsymbol{E}_c$. Thus, the phase-conjugate wave is often referred to as the time-reversed wave.

To appreciate the property of phase conjugation, we consider the propagation of a plane wave through a distorting medium and incident upon a phase-conjugate mirror, as shown in Fig. 1.2. When the plane wave through the distorting medium, as a result of the nonuniformity of the refractive index n (x, y, z) of the distorting medium, the wave fronts of the transmitted wave are no longer planar [Fig 1.2(a)]. The transmitted wave is redirected by a phase-conjugate mirror. The generated conjugate beam inputs again the distorting medium. Note that the conjugate beam returns to the same plane wave [Fig. 1.2(b)]. This indicates that phase-conjugate

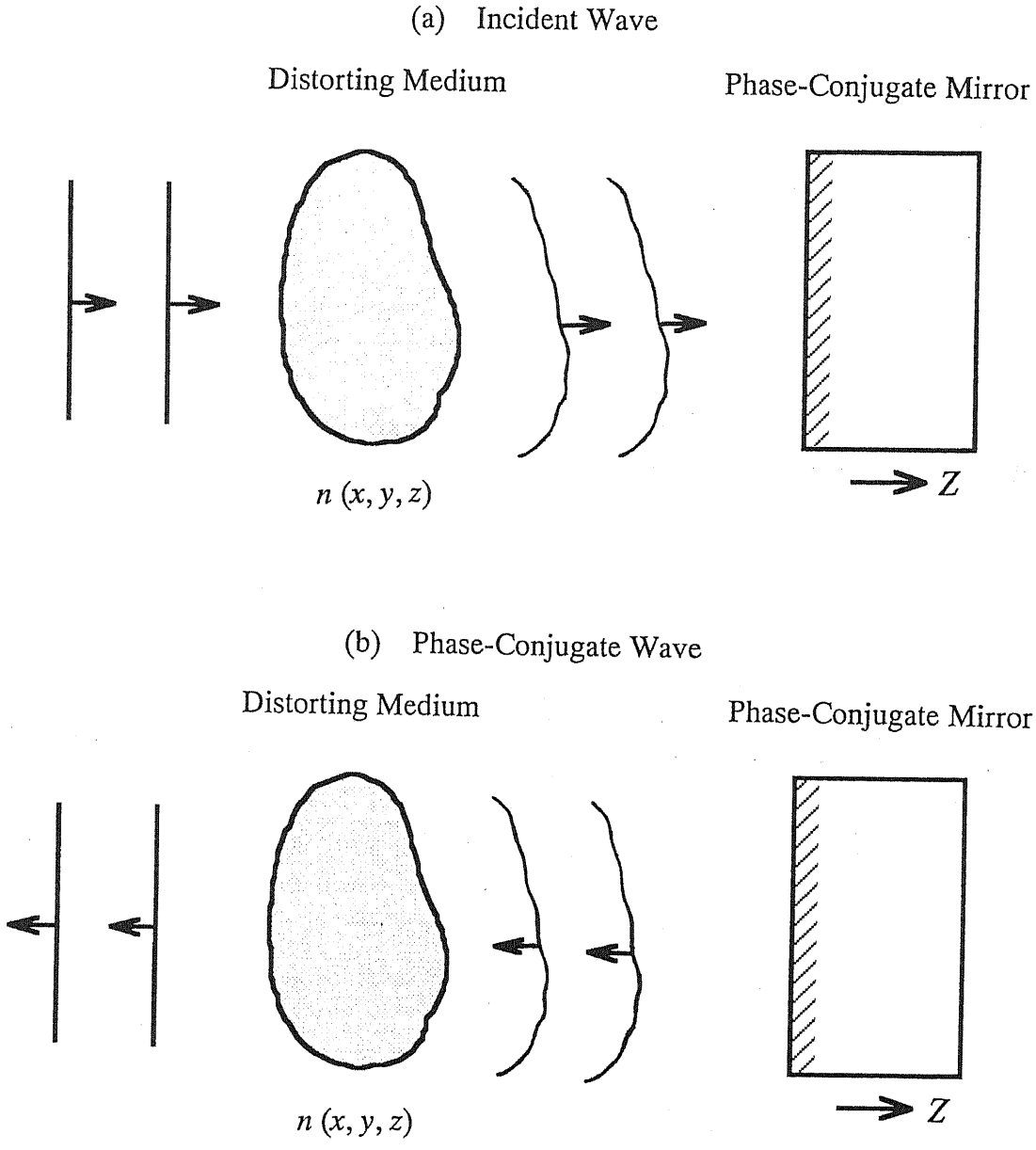

Fig. 1.2. (a) An plane wave transmitted through a distorting medium (the wave fronts of the transmitted beam are no longer planar) and incident upon a phase-conjugate mirror. (b) Phase-conjugate wave generated by the phase-conjugate mirror retraces the path of the incident beam and transmits through the distorting medium. The plane wave fronts are restored.

waves have retroreflection and wavefront reconstruction properties.

Nonlinear optical phase conjugation was first observed in the backward scattered light produced by stimulated Brillouin scattering (SBS).[18] No pump beams are required for phase conjugation by SBS. However, because of the SBS growth from the scattered noise, the intensity of the incident wave must exceed a threshold value (> 10^9 W/cm^2) for the process to occur. Three-wave mixing in asymmetric crystals can also yield wave-front reversed replicas.[19,20] However the phase matching condition restricts the angular field of view of the input wave to very small values. This restriction is eliminated in phase conjugation by four-wave mixing.[21-23] In photorefractive media, phase conjugate based on four-wave mixing occurs at a much less operating intensity as compared with other nonlinear optical processes. By far potorefractive crystals, such as $BaTiO_3$, $Sr_{0.75}Ba_{0.25}Nb_2O_6$ (SBN), $Bi_{12}SiO_{20}$ (BSO) $(K_{0.5}Na_{0.5})_{0.2}(Sr_{0.61}Ba_{0.39})_{0.9}Nb_2O_6$ (KNSBN), are the most efficient media for the generation of phase-conjugate waves. In 1980, Feinberg *et al.* observed first continuous-wave self-oscillation in an optical resonator formed by phase-conjugate mirror and a normal mirror.[24] White *et al.* demonstrated several optical oscillator configurations in 1982.[25] In 1982, Feinberg demonstrated a versatile and effective self-pumped phase-conjugate mirror (SPPCM) in a photorefractive $BaTiO_3$ crystal, known as the cat mirror, which was self-starting and did not need any external pump beam or cavities.[26] Since the SPPCM was formed in a $BaTiO_3$ crystal, SPPCM has been also observed in other photorefractive crystals, such as SBN, KNSBN, and so on. The theory of SPPCM has been also presented by Macdonald and Feinberg.[27] Many researchers have made great efforts to increase the phase-conjugate reflectivity and enhance the response speed of SPPCM. Moreover, they revealed the dynamic properties of SPPCM. However, the dynamic instability of SPPCM, which is frequently encountered in experiments, continues to be a problem. Many studies

have shown that the dynamic instability of SPPCM are regular fluctuation, irregular fluctuation, or optical chaos of four-wave mixing,[28-33] while others have shown that the dynamic instability depends on such conditions of the incident beam as incident position and incident power.[33-35] To further investigate origin of the dynamic instability and eliminate this instability are critical to SPPCM applications.

In 1987, Weiss *et al.* reported first a double phase-conjugate mirror (DPCM) in a $BaTiO_3$ crystal based on four-wave mixing, which might carry different spatial images.[36] In 1987, Eason *et al.* showed the mutually incoherent beam coupler, which two mutually incoherent beams simultaneously incident on the same side of a $BaTiO_3$ crystal.[37,38] In 1988, Ewbank reported and explained the bird-wing phase conjugator in a $BaTiO_3$ crystal which involved more than one interactive region and reflection at the surface of the crystal.[39] As various different incident geometrical DPCMs were demonstrated, the theoretical models of DPCMs were also proposed and analyzed.[40,41] However, the efficiencies of reported DPCMs are not too high. The performance enhancement of DPCM has been required for its applications. Recently, a stable high-efficiency DPCM in a Cu-doped $(K_{0.5}Na_{0.5})_{0.2}(Sr_{0.61}Ba_{0.39})_{0.9}Nb_2O_6$ (Cu:KNSBN) crystal was first reported by Gao *et al.*[42] However how to form a high-performance DPCM in a photorefractive crystal is a problem yet. For crystals with different absorption coefficients, the optimum incident geometries for forming an efficient DPCM also need to be revealed.

Photorefractive materials with their unique properties of real-time response and low-intensity operation provide promising candidates for many applications, such as optical information processing, optical computing, and optical communication.[43-46] Real-time image processing via four-wave mixing in a photorefractive medium was demonstrated by White and Yariv in 1980.[47] They used optical four-wave mixing in a BSO crystal to perform image convolution and correlation. The use of a phase-

conjugate mirror (PCM) to project images was first reported by Levenson in 1980.[48] However, when projecting three-dimensional (3D) images, PCMs bring inconvenient viewing, because PCMs produce real pseudoscopic images with their perspective inversion. The real-time orthoscopic 3D image projection using the feedback phase-conjugate setup was demonstrated in 1991.[49] However, the phase-conjugate reflectivity of the feedback phase-conjugate setup was not high. Its performance is also unstable.[49,50]

Other exciting applications of photorefractive materials are for optical computing and optical communication. Interconnection devices are the basics devices in optical computing and optical communication, which have drawn great attention. Yeh *et al.* reported a kind of method reconfigurable optical interconnection using dynamic holograms in photorefractive crystal in 1988.[51] The optical conjugation is the most prospective means to realize the dynamic interconnection. The dynamic interconnection device has self-adaptive and fault-tolerant properties. Weiss *et al.* proposed the photorefractive dynamic optical interconnections.[7,13] Schamschula *et al.* presented the adaptive interconnection for the message-bearing light irradiated onto the detector.[14] Recently, Chiou *et al.* reported the photorefractive spatial mode converter.[17] However, all-optical switching dynamic interconnection and all-optical routing switching dynamic interconnection have not be reported yet.

The properties of three kinds of general photorefractive crystals are listed in Table 1.1. In the previous researches, most of studies were carried out using $BaTiO_3$ and SBN crystals. Although $BaTiO_3$ crystal has a very large electrooptic coefficient (r_{42}), it suffers from an inconvenient Curie temperature of about 10°C.[52] Once the temperature is lower than the critical temperature, phase transition of the crystal quickly occurs, after which the crystal does not recover its former state. For this reason, it is not convenient for practical use. The electrooptic coefficients of SBN

Table 1.1. Comparison of the properties for three kinds of general photorefractive crystals

Crystal	$BaTiO_3$	SBN $Sr_{0.61}Ba_{0.39}Nb_2O_6$	Cu:KNSBN Cu-doped $(K_{0.5}Na_{0.5})_{0.2}(Sr_{0.61}Ba_{0.39})_{0.9}Nb_2O_6$ ~0.01-0.06 wt % doped CuO
Curie temperature T_c (°C)	$10 < T < 128$	75	140
Electrooptic coefficient (10^{-12} m/V)	$r_{13} = 19.5$ $r_{33} = 97$ $r_{42} = 1640$	$r_{13} = 47$ $r_{33} = 235$	$r_{13} = 50$ $r_{33} = 270$ $r_{42} = 400$
Index of refraction ($\lambda = 514.5$ nm)	$n_o = 2.43$ $n_e = 2.36$	$n_o = 2.33$ $n_e = 2.30$	$n_o = 2.30$ $n_e = 2.27$
Crystal growth	difficult	easy	easy

crystal are not large and the response speed is slow.[52] Therefore, in recent years, Cu-doped KNSBN crystal has attracted much attention. Cu:KNSBN crystal has large electrooptic coefficients (r_{42} and r_{33}) and is easy to grow.[53] In Cu:KNSBN crystal, there is no inconvenient critical temperature in the usual atmospheric temperature range. Thus Cu:KNSBN crystal has the advantage of convenient usability. In this thesis, all studies are investigated using Cu:KNSBN crystals.

1.2 Outline of This Thesis

In the present thesis, the dynamic instability of a SPPCM is investigated by the theory and the experiment. Then how to form a high-performance DPCM is presented. For crystals with different absorption coefficients, the optimum incident geometries are also studied. The latter part of the thesis is devoted to applications of PCMs. The concrete organization is as follows.

Chapter 1 is this introduction, which provide an review of optical phase conjugation and the outline of this thesis.

Chapter 2 is devoted to further study on the dynamic instability of a SPPCM in a Cu:KNSBN crystal. The origin and elimination of dynamic instability of the SPPCM are proved and discussed by the theory and the experiment.

In chapter 3, how to form a high-performance DPCM with a modified-bridge incident geometry in a Cu:KNSBN crystal is described. A high phase-conjugation transmissivity with a high stability is observed under Brewster angle incidence. Chapter 4 concerns with the formation of high-efficiency DPCMs with a bridge incident geometry in Cu:KNSBNs. The optimum incident geometries of DPCMs with the Cu:KNSBN crystals of different absorption coefficients are observed and

discussed.

Chapter 5 deals with the formation of multiple PCM consisting of a SPPCM and a bridge DPCM in a Cu:KNSBN crystal. Two phase-conjugate operations on an input light wave are described. The transmissivities and stability of the multiple PCM are investigated. The spatial fidelity of the multiple PCM and the real-time orthoscopic three-dimensional image projection using the multiple PCM are also observed.

Chapter 6 addresses all-optical switching dynamic interconnection with multiple DPCMs in a Cu:KNSBN crystal. The switching optical dynamic interconnection between two light beams using two DPCMs is proposed. Further, 1 × 2 all-optical routing switching dynamic interconnection is investigated with multiple DPCMs.

Last, the summary for the thesis is presented. The suggestions for further study are also given.

References

1. R. A. Fisher, *Optical Phase Conjugation,* Academic, New York, (1983).
2. A. Yariv, *Optical Electronics* (Fourth Edition), Saunders College Publishing, (1991).
3. P. Yeh, Introduction to Photorefractive Nonlinear Optics, John Wiley and Sons, Inc. (1993).
4. M. Gower and D. Proch, *Optical Phase Conjugation,* Springer-Verlag, (1994).
5. P. Gunter and J. -P. Huignard, *Photorefractive Materials and Their Application II,* Springer-Verlag, (1989).
6. J. Feinberg, *Opt. Lett.* **8,** 569 (1983).
7. B. Fischer, S. Sternklar, and S. Weiss, *IEEE J. Quantum Electron.* **QE-25,** 550 (1989).
8. S. Sternklar, S. Weiss, and B. Fischer, *Opt. Eng.* **26,** 423 (1987).
9. R. J. Anderson, E. J. Sharp, G. L. Wood, and G. J. Salamo, *Appl. Opt.* **35,** 854 (1996).
10. J. M. Yarrison-Rice, E. J. Sharp, G. L. Wood, and R. R. Neurgaonkar, *Appl. Opt.* **35,** 1904 (1996).
11. J. Shamir, H. J. Caulfield, and B. M. Hendrickson, *Appl. Opt.* **27,** 2912 (1988).
12. Q. C. He, J. Shamir, and J. G. Duthie, *Appl. Opt.* **28,** 306 (1989).
13. S. Weiss, M. Segev, S. Sternklar, and B. Fischer, *Appl. Opt.* **27,** 3422 (1988).
14. M. P. Schamschula, H. J. Caulfield, and C. M. Verber, *Opt. Lett.* **16,** 1421 (1991).
15. A. Chiou, P. Yeh, C. Yang, and C. Gu, *IEEE Photonics Technol. Lett.* **7,** 789 (1995).

16. C. Medrano, M. Zgonik, P. Bernasconi, and P. Gunter, *Opt. Commun.* **128,** 177 (1996).

17. A. Chiou, P. Yeh, C. Yang, and C. Gu, *Opt. Lett.* **20,** 1125 (1995).

18. B. Ya. Zel'dovich, V. I. Popovivhec, V. V. Ragul'skii, and F. S. Faizullov, *Sov. Phys. JEPT* **15,** 109 (1972).

19. A. Yariv, *Appl. Phys. Lett.* **28,** 88 (1976).

20. A. Yariv, *Opt. Commun.* **21,** 49 (1977).

21. A. Yariv and D. M. Pepper, *Opt. Lett.* **1,** 16 (1977).

22. R. W. Hellwarth, *J. Opt. Soc. Am.* **67,** 1 (1977).

23. M. Bloom and G. C. Bjorklund, *Appl. Phys. Lett.* **31,** 592 (1977).

24. J. Feinberg and R. W. Hellwarth, *Opt. Lett.* **5,** 519 (1980).

25. J. O. White, M. Cronin-Golomb, B. Fischer, and A. Yariv, *Appl. Phys. Lett.* **40,** 450 (1982).

26. J. Feinberg, *Opt. Lett.* **7,** 486 (1982).

27. K. R. MacDonald and J. Feinberg, *J. Opt. Soc. Am.* **73,** 5488 (1983).

28. A. M. C. Smout, R. W. Eason, and M. C. Gower, *Opt. Commun.* **59,** 77 (1986).

29. D. J. Gauthier, P. Narum, and R. W. Boyd, *Phys. Rev. Lett.* **58,** 1640 (1987).

30. A. V. Nowak, T. R. Moore, and R. A. Fisher, *J. Opt. Soc. Am.* **B 5,** 1864 (1988).

31. T. Rauch, C. Denz, and T. Tschudi, *Opt. Commun.* **88,** 160 (1992).

32. P. M. Jeffrey and R. W. Eason, *J. Opt. Soc. Am.* **B 11,** 476 (1994).

33. P. Gunter, E. Voit, M. Z. Zha, and J. Albers, *Opt. Commun.* **55,** 210 (1985).

34. M. C. Gower and P. Hribek, *J. Opt. Soc. Am.* **B 5,** 1750 (1988).

35. A. K. Majumdar and J. L. Kobesky, *Opt. Commun.* **75,** 339 (1990).

36. S. Weiss, S. Sternklar, and B. Fischer, *Opt. Lett.* **12,** 114 (1987).

37. R. W. Eason and A. M. C. Smout, *Opt. Lett.* **12,** 51 (1987).

38. A. M. C. Smout and R. W. Eason, *Opt. Lett.* **12,** 498 (1987).

39. M. D. Ewbank, *Opt. Lett.* **13,** 47 (1988).

40. Q. C. He, *IEEE J. Quantum Electron.* **24,** 2507 (1988).

41. P. Yeh, T. Y. Chang, and M. D. Ewbank, *J. Opt. Soc. Am.* **B 5,** 1743 (1988).

42. X. Gao, A. Sasaki, and Y. Zheng, *Jpn. J. Appl. Phys.* **32,** L1654 (1993).

43. H. Soffer, G. J. Dunning, Y. Owechko, and E. Marom, *Opt. Lett.* **11,** 118 (1986).

44. A. Yariv and S. K. Kwong, *Opt. Lett.* **11,** 186 (1986).

45. D. Z. Anderson, *Opt. Lett.* **11,** 45 (1986).

46. H. J. Caulfield, J. Shamir, and Q. C. He, *Appl. Opt.* **26,** 2291 (1987).

47. J. O. White and A. Yariv, *Appl. Phys. Lett.* **37,** 5 (1980).

48. M. D. Levenson, *Opt. Lett.* **5,** 182 (1980).

49. N. A. Vainos and M. C. Gower, *J. Opt. Soc. Am.* **B 8,** 2355 (1991).

50. M. Zhao and I. Yamaguchi, *Opt. Commun.* **112,** 163 (1994).

51. P. Yeh, A. E. T. Chiou, and J. Hong, *Appl. Opt.* **27,** 2093 (1988).

52. M. D. Ewbank, R. R. Neurgaonkar, and W. K. Cory, *J. Appl. Phys.* **62,** 374 (1987).

53. X. Yue, X. Lu, Y. Song, Z. Shao, D. Sun, Q. Jiang, and H. Chen, *Appl. Phys.* **B 53,** 319 (1991).

Chapter 2

Origin and Elimination of Dynamic Instability in a Self-Pumped Phase-Conjugate Mirror (SPPCM)

The origin and the elimination of dynamic instability are further studied in a self-pumped phase-conjugate mirror (SPPCM) of a Cu:KNSBN crystal. Experimental results prove that the dynamic instability of the SPPCM arises from the competition between the self-generated fanning effect and SPPCM formation. The theory and experiment show that the ordinary-polarized component of a partially extraordinary-polarized incident light beam can act to decrease the self-generated fanning effect of the photorefractive crystal. The dynamic instability of the SPPCM is eliminated by restraining the self-generated fanning effect with a partially extraordinary-polarized incident light beam.

2.1 Introduction

The self-pumped phase-conjugate mirror (SPPCM), or called the cat mirror, has been extensively studied since it was observed by Feinberg in 1982.[1] The SPPCM

was self-starting and did not need any external pump beam or cavities. The SPPCM has attracted special interest for a number of applications, such as correction of the wave-front distortion, optical image processing, optical interferometer,[2,3] and so on. However, the dynamic instability of the SPPCM, which is frequently encountered in experiments, continues to be a problem. The elimination of this instability is critical to SPPCM applications. Many researchers have proposed that the dynamic instability of the SPPCM is regular fluctuation, irregular fluctuation, or optical chaos of four-wave mixing,[4-9] while others have shown that the dynamic instability depends on the incident conditions (incident angle, incident position and incident beam diameter) of the incident beam.[9-11] The behavior of the dynamic instability seems to be a complex problem. The origin and the elimination of dynamic instability in a SPPCM had been advanced by Gao.[12] In Ref. 12, it was directed that the origin of the dynamic instability in a SPPCM is the competition between the self-generated fanning process and the SPPCM formation. The dynamic instability can be eliminated by rotating the polarized direction of the incident light. However, the experimental study to prove the origin of the dynamic instability and the theoretical analysis to eliminate the dynamic instability of the SPPCM have not been presented.

In this chapter, the origin and the elimination of the dynamic instability are further studied in a SPPCM.[13] A theory of two-wave mixing is described, which is used to explain the self-generated fanning effect in photorefractive crystal SPPCM. The dynamic instability of the SPPCM is observed. We prove experimentally that the origin of the dynamic instability arises from the competition between the self-generated fanning effect and SPPCM formation. We further give the theoretical explanation why the partially extraordinary-polarized incident light beam can eliminate the dynamic instability of the SPPCM.

2.2 Fanning Effect in Photorefractive Crystal

The photorefractive effect is an optical phenomenon in some electro-optic crystal (including $LiNbO_3$, $BaTiO_3$, $KNbO_3$, SBN, KNSBN, BSO, etc.) where the local index of refraction is changed by the spatial variation of the light intensity.[14] The spatial index variation leads to the distortion of the wave front. Such an effect was referred to as "optical damage". The optical damage is driven by the gradient of the light intensity.

The photorefractive effect is believed to arise from optically generated charge carriers which migrate when the photorefractive crystal is illuminated by the incident light of spatial non-uniformity. Migration of the charge carriers due to diffusion, drift, and the photovoltaic effect produces a space-charge separation, which then gives rise to a strong space-charge field. The space-charge field induces a refraction index change via the electro-optic effect (Pockels effect).

When a light beam is incident on a photorefractive crystal, the scattering is occurred because of index inhomogeneity and impurities in the crystal. The scattered light is asymmetrical with respect to the incident beam. If the incident beam has a finite transverse cross section, the scattered beam will have an overlap with the incident beam. Since the scattered beam has a large number of spatial components, the overlap leads to the formation of a large number of photo-induced gratings. Depending on the orientation of the crystal, some of the spatial components may be amplified by the incident beam via the energy coupling in two-wave mixing. This is known as self-generated fanning effect.

We now consider the interaction of two laser beams inside a photorefractive crystal (see Fig. 2.1). Let the electric field of the two optical waves be written

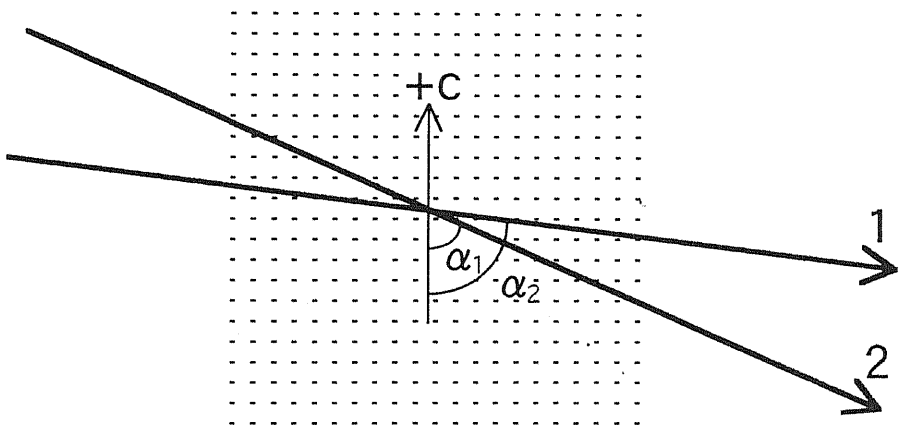

Fig. 2.1. Configuration of two-wave mixing inside a photorefractive crystal.

$$E_j = A_j \exp[i(\boldsymbol{k}_j \cdot \boldsymbol{r} - \omega t)], \quad j = 1,2 \tag{2.1}$$

where A_1, A_2 are the wave amplitudes, ω is the angular frequency, and $\boldsymbol{k}_1$, $\boldsymbol{k}_2$ are the wave vectors. For the two beams of the same frequency, a stationary interference pattern is formed. In response to the interference pattern of the optical waves, the photorefractive medium evolves a space-charge field that, in turn, gives rise to a refractive index grating. The spatial evolution of the electric field may be approached using the coupled-wave theory. The basic photorefractive two-wave mixing equations are given by (neglecting absorption)[2,15-17]

$$\frac{\partial A_1(z,t)}{\partial z} = -g^*(z,t)A_2(z,t), \tag{2.2}$$

$$\frac{\partial A_2(z,t)}{\partial z} = g(z,t)A_1(z,t). \tag{2.3}$$

In steady state, the grating g is

$$g = \gamma \frac{A_1(z)A_2^*(z)}{I}, \tag{2.4}$$

where I is the total intensity, and γ is the coupling coefficient between the beams. We can see that the grating g is proportional to the coupling coefficient γ in steady state. The coupling coefficient γ is written by[1,2,18-20]

$$\gamma = \frac{\omega}{2nc}\frac{r_{\text{eff}}E}{\cos\left(\frac{\alpha_1 - \alpha_2}{2}\right)}, \tag{2.5}$$

where angles α_1 and α_2 are given in Fig. 2.1, the quantity E has unit of electric field, and, when there is no uniform dc electric field in the crystal, it is given by

$$E = \frac{k_B T}{q}\frac{k_g}{1+(k_g/k_0)^2}\boldsymbol{P}_1 \cdot \boldsymbol{P}_2^*, \tag{2.6}$$

where $\boldsymbol{P}_1$ and $\boldsymbol{P}_2$ are unit vectors describing the polarization states of the waves, k_g is the signed magnitude of the grating wave vector $\boldsymbol{K}_g$ ($\boldsymbol{K}_g = \boldsymbol{k}_2 - \boldsymbol{k}_1$), it is written by

$$k_g = 2\left(\frac{n\omega}{c}\right)\sin\left(\frac{\alpha_1 - \alpha_2}{2}\right), \tag{2.7}$$

and the parameter k_0 is determined by the charge number density N according to

$$k_0 = \left(\frac{Nq^2}{\varepsilon\varepsilon_0 k_B T}\right)^{1/2}, \tag{2.8}$$

where $k_B T$ is the thermal energy, q is the charge of the carriers, ε_0 is the permittivity of free space, and ε is the effective dielectric constant in the direction of $\boldsymbol{K}_g$, it is given by

$$\varepsilon = K_g \cdot \boldsymbol{\varepsilon} \cdot K_g / k_g^{\,2}, \tag{2.9}$$

$\boldsymbol{\varepsilon}$ is the dielectric tensor. For crystals of point group 4 mm, such as $BaTiO_3$, SBN, Cu:KNSBN, the effective Pockels coefficient r_{eff} in Eq. (2.5) for ordinary-polarized light is given by

$$r_{\text{eff}} = n_o^{\,4} r_{13} \sin\left(\frac{\alpha_1 + \alpha_2}{2}\right). \tag{2.10}$$

For extraordinary-polarized light, the effective Pockels coefficient r_{eff} is

$$\begin{aligned} r_{\text{eff}} = \{ & n_e^{\,4} r_{33} \sin\alpha_1 \sin\alpha_2 + 2 n_e^{\,2} n_o^{\,2} r_{42} \cos^2[(\alpha_1 + \alpha_2)/2] \\ & + n_o^{\,4} r_{13} \cos\alpha_1 \cos\alpha_2 \} \sin[(\alpha_1 + \alpha_2)/2], \end{aligned} \tag{2.11}$$

where n_o and n_e are the ordinary and extraordinary refractive indexes, respectively, r_{33}, r_{42} and r_{13} are the electrooptic coefficients. Thus, we can see that the coupling coefficient γ depends on the angles of the incident light beams and is proportional to the electrooptic coefficients. The electrooptic coefficients of photorefractive crystals ($BaTiO_3$, SBN, Cu:KNSBN) have been listed in Table1.1. According to Eqs. (2.11) and (2.5), these photorefractive crystals have large two-wave mixing coupling coefficients for extraordinary-polarized light. Thus, the self-generated fanning effect by two-wave mixing is generated in these photorefractive crystals. Figure 2.2 shows self-generated fanning of a Cu:KNSBN crystal under the incidence of extraordinary-polarized light beam. The Cu:KNSBN crystal has the strong self-generated fanning effect.

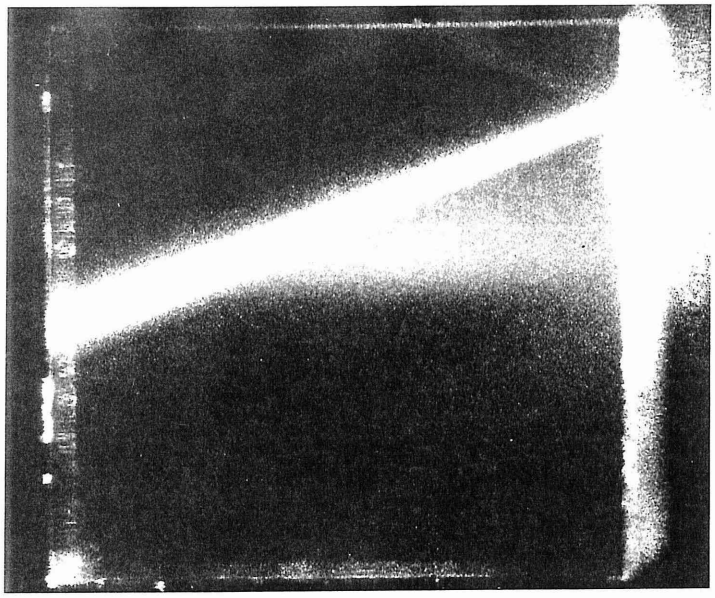

Fig. 2.2. Self-generated fanning in a Cu:KNSBN crystal.

2.3 Experimental Certification on the Origin of Dynamic Instability in a Cu:KNSBN SPPCM

The general experimental setup of a SPPCM is shown in Fig. 2.3. A photorefractive Cu:KNSBN crystal (6 mm × 6 mm × 6 mm) is illuminated by a pump beam from an argon-ion laser at λ = 514.5 nm. The incident beam diameter is 1.6 mm. The polarized direction of the incident light can be adjusted by rotation of the half-wave plate. The angle scale of the polarization of the incident light is defined as $\Phi = 0°$ corresponding to the extraordinary-polarized direction and $\Phi = 90°$ corresponding to the ordinary-polarized direction. When the polarized incident light is neither extraordinary nor ordinary, that is, $\Phi \neq 0°$ and $\Phi \neq 90°$, the incident light is called a partially extraordinary-polarized light beam. In normal SPPCM experiments the incident light beam is extraordinary polarized because the extraordinary-polarized light corresponds to the largest photorefractive effect. Figure 2.4 shows the dynamic instability of the Cu:KNSBN SPPCM under extraordinary-polarized light incidence. Here the dynamic instability is an irregular large fluctuation. For the three states (points A, B, C in Fig. 2.4) of dynamic instability, photographs of these SPPCM states were taken, as shown in Figs. 2.5(a), 2.5(b), and 2.5(c), respectively. In SPPCM experiments, two self-generated phenomena exist when a laser light beam illuminates a photorefractive crystal. One is self-generated fanning, and the other is the self-pumped four-wave mixing that corresponds to the SPPCM. In photorefractive crystals, most of incident light is transformed into self-generated fanning in some cases. It should be noted that the self-generated fanning affects self-pumped phase-conjugate mirrors.[21,22] The SPPCM formation and the self-generated fanning effect are shown in Fig. 2.6. G1 corresponds to the grating of the self-generated fanning, and G2 corresponds to the grating of the SPPCM.

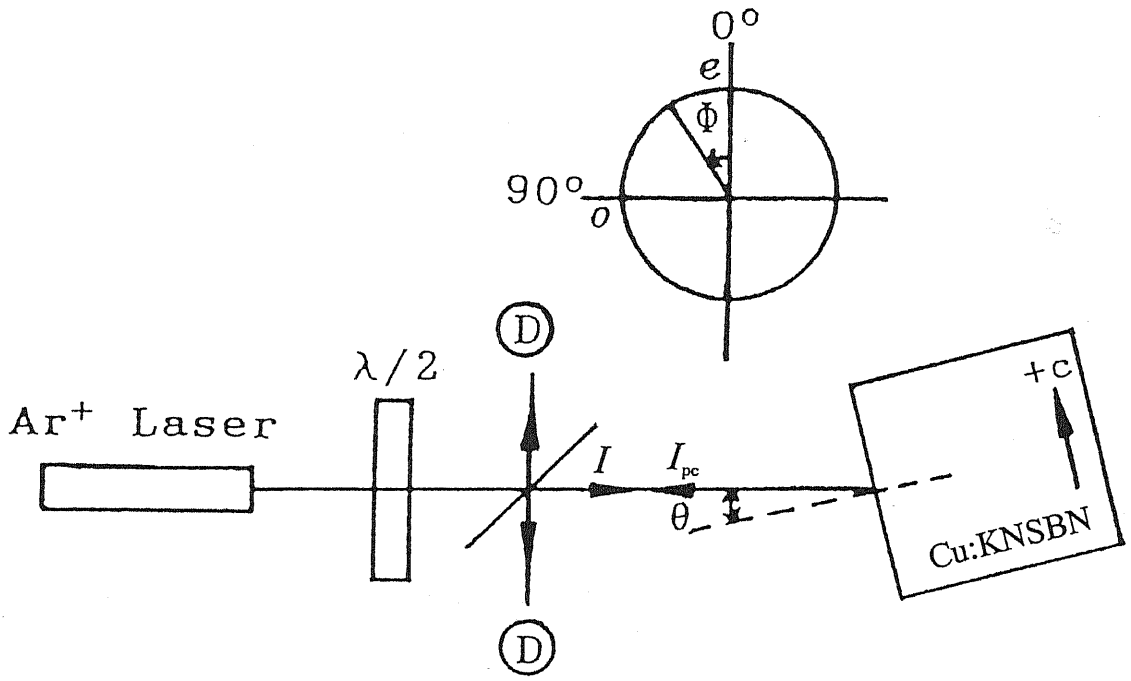

Fig. 2.3. Experimental arrangement of the Cu:KNSBN crystal SPPCM. θ, incident angle; Φ, polarization angle between the polarized direction of incident light and the extraordinary-polarized direction; e and o, extraordinary and ordinary light, respectively; λ/2, half-wave plate; D's, detectors.

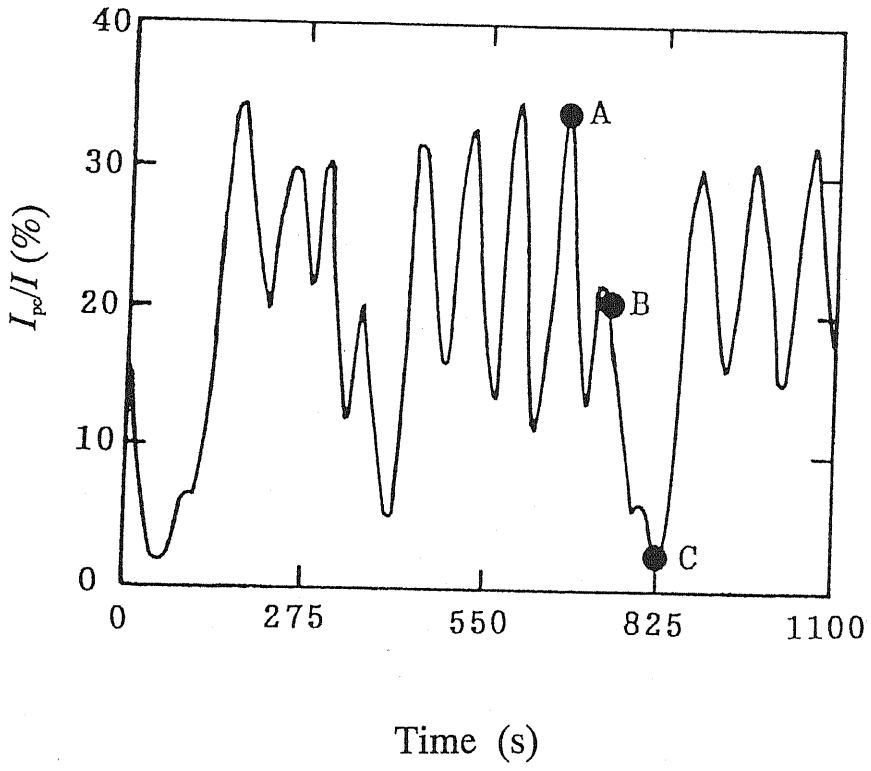

Fig. 2.4. Observed dynamic instability of the SPPCM under extraordinary-polarized light incident ($\Phi = 0°$). Here the incident angle θ is 35°, and the incident light power is 5 mW. The ordinate corresponds to the I_{pc}/I percentage.

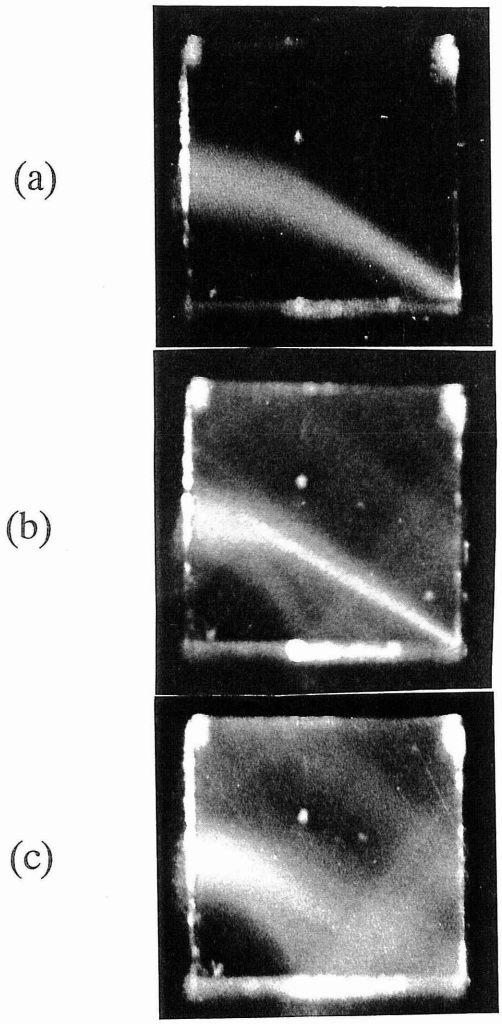

Fig. 2.5. Photographs of the SPPCM in three different states of dynamic instability. (a), (b), and (c) correspond to points A, B, and C, respectively, of Fig. 2.4.

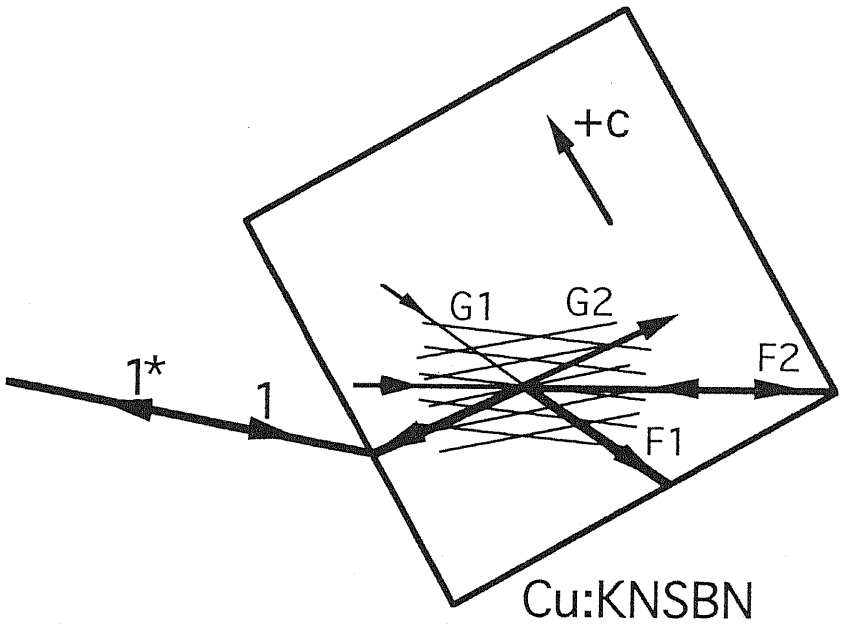

Fig. 2.6. Schematic of the competition between the SPPCM formation and the self-generated fanning effect. G1, the grating of the self-generated fanning; G2, the grating of SPPCM.

Self-generated fanning F1 propagates in the maximum gain direction. Fanning F2 of the SPPCM propagates in corner direction of the crystal. When the gains of the two effects are comparable, strong competition between the self-generated fanning effect and the SPPCM formation takes place. We believe that the competition of the two set gratings is an unstable process that leads to the dynamic instability of the SPPCM. Figure 2.5 clearly shows the competition process. In Fig. 2.5(a) the SPPCM formation has superiority in the competition, thus the phase-conjugate light is in the peak point A of Fig. 2.4. In Fig. 2.5(b) the SPPCM is weaker, and the self-generated fanning is clearly shown, with the phase-conjugate light decreasing to point B of Fig. 2.4. In Fig. 2.5(c) the self-generated fanning apparently has superiority, with the phase-conjugate light in the valley point C of Fig. 2.4. This clearly shows that the dynamic instability of the SPPCM arises from the competition between the self-generated fanning effect and the SPPCM formation.

2.4 Theoretical Analysis and Experimental Study on the Elimination of Dynamic Instability in a SPPCM

Let us examine Eq. (2.4) for the grating amplitude in two-wave mixing. The total intensity I is

$$I = I_1 + I_2, \tag{2.12}$$

I_1 and I_2 are the intensities of two mixing wave, respectively. Thus Eq. (2.4) is written

$$g = \gamma \frac{A_1(z)A_2^*(z)}{I_1 + I_2}. \tag{2.13}$$

We can see that the grating g is not only proportional to the coupling coefficient γ, but also inverse proportional to the total intensity I of two mixing wave. In the two-wave mixing, if we add a background beam (by a laser beam which is mutually incoherent to the two mixing waves), the total intensity can be written as

$$I = I_1 + I_2 + I_0, \tag{2.14}$$

where I_0 is the intensity of the added background beam. Equation (2.4) is now written as

$$g = \gamma \frac{A_1(z)A_2^*(z)}{I_1 + I_2 + I_0}. \tag{2.15}$$

On comparing Eq. (2.13) and Eq. (2.15), we find that increasing I while keeping the coupling coefficient γ constant is equivalent to reducing γ while keeping I constant. In other words, in the two-wave mixing, when a background light beam of mutually incoherent to the two mixing waves is inputted simultaneously. The gain of the two-wave mixing is decreased. Of course, if this background beam is in any way mutually coherent with the two mixing waves, then it will also couple with both waves and change the entire dynamics. To avoid this the background light should be completely incoherent with the interacting beams, and it could be a different polarized light with the two mixing waves. The gain of two-wave mixing can be reduced by simply introducing an incoherent background beam, that is, the self-generated fanning effect in a SPPCM can be reduced by introducing an incoherent background beam. To further prove the above conclusions and to eliminate the dynamic instability, we carried out experiments exploring the means to restrain the

self-generated fanning effect and to eliminate the dynamic instability by using the partially extraordinary-polarized incident light of which the ordinary-polarized component plays the role of incoherent background beam. In Ref. 23 the ordinary-polarized light was used as a tool to erase the grating of a double phase-conjugate mirror. Here we investigate the diffraction-efficiency change of the self-generated fanning when the polarization angle of the incident light beam is rotated, using the experiment arrangement shown in Fig. 2.7. In this experiment the self-generated fanning takes place only in the extraordinary-polarized component. We define the diffraction efficiency η of self-generated fanning as

$$\eta = \frac{I_{ef}}{\rho I_{ein}} = \frac{\rho I_{ein} - I_{eout}}{\rho I_{ein}}, \tag{2.16}$$

where ρ is the light loss in the light path. Figure 2.8 shows the diffraction efficiency η as a function of the polarization angle Φ. In Fig. 2.8 the diffraction efficiency clearly decreases when polarization angle Φ increases. This means that the self-generated fanning effect can be effectively weakened when the partially extraordinary-polarized incident light replaces the extraordinary-polarized incident light. As above described, the self-generated fanning effect is reduced by introducing an incoherent background beam (the ordinary-polarized component of a partially extraordinary-polarized light).

Using the experimental arrangement of Fig. 2.3, under the same incident conditions as those of Fig. 2.4, we observed the dynamic instability of the SPPCM when the polarization direction of the partially extraordinary-polarized light was changed, with the results shown in Fig. 2.9. In our experiment, even though the incident light is partially extraordinary polarized, the observed phase-conjugate light

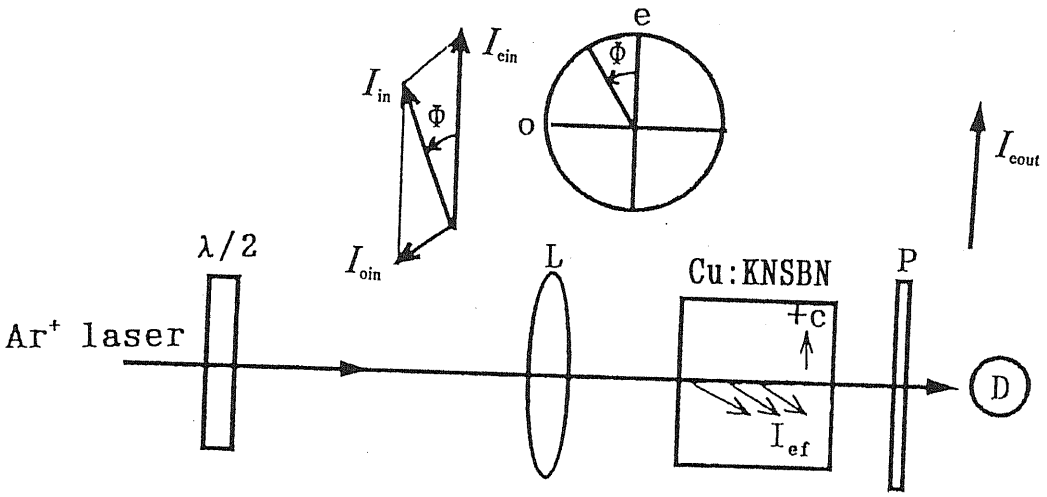

Fig. 2.7. Experimental arrangement for investigating the diffraction-efficiency change of self-generated fanning as a function of the polarization direction of the incident light that is vertically incident upon the surface of the Cu:KNSBN crystal. The incident light power is 5 mW, the focus of the lens is 18.5 cm, and the incident beam diameter is 1.1 mm. P, polarizer; D, detector.

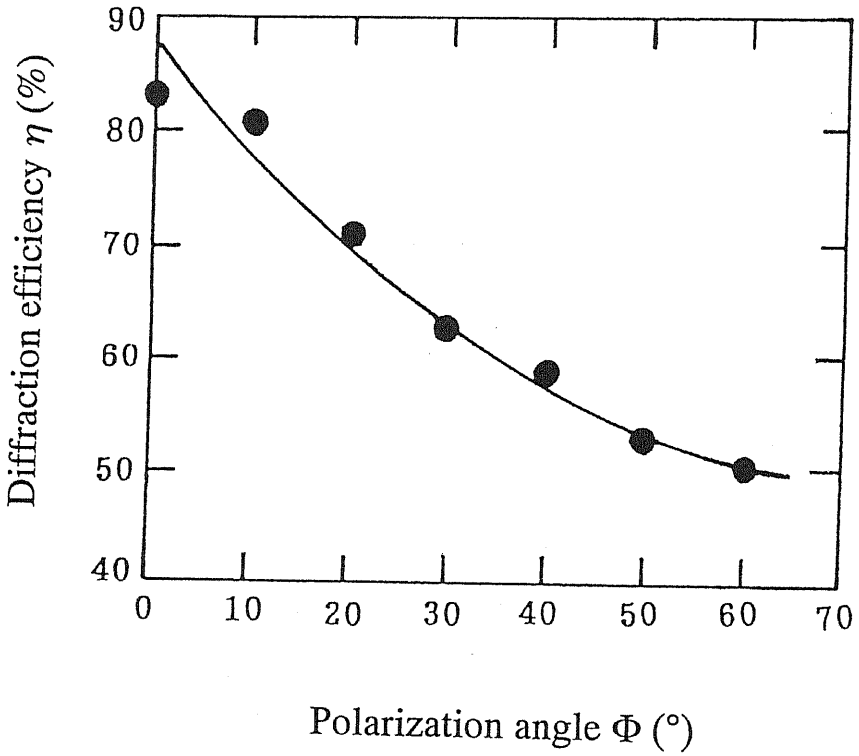

Fig. 2.8. Diffraction efficiency of self-generated fanning as a function of the polarization angle of the incident light.

is only extraordinary-polarized light. This is because ordinary-polarized light does not satisfy the Bragg-diffraction conditions of the grating that forms the SPPCM. The ordinary-polarized component transmits the interaction region of the SPPCM and plays only the role of erasing the grating of self-generated fanning. In Fig. 2.9(a), when Φ is 26°, the stability of the SPPCM is improved compared with that of Fig. 2.4. Further increasing Φ to 35°, that is, increasing the ordinary-polarized component, we observed that the dynamic instability is effectively eliminated [see Fig. 2.9(b)]. In this case the self-generated fanning effect in the SPPCM is effectively restrained by the ordinary-polarized component of the partially extraordinary-polarized incident light. The SPPCM formation wins the competition and maintains stable operation. Also, although the phase-conjugate reflectivity I_{pc}/I dose not increase compared with the peak value in Fig. 2.4, the ratio I_{pc}/I_e of the phase-conjugate light and the extraordinary-polarized component of the incident light is apparently increased. This means that the gain of the SPPCM is not decreased because the gain of the SPPCM is considered to be in the saturated state, and since the self-generated fanning effect is restrained, previous self-generated fanning light is coupled into the SPPCM loop. These experimental results not only show that the dynamic instability of SPPCM can be eliminated by use of partially extraordinary-polarized incident light instead of extraordinary-polarized light but also further prove that the dynamic instability of the SPPCM originates from the competition between the self-generated fanning effect and the SPPCM formation.

The results described above are universal for any incident condition. For any unstable-operation state of the SPPCM under extraordinary-polarized light incidence, the dynamic instability can be eliminated by rotating the half-wave plate.

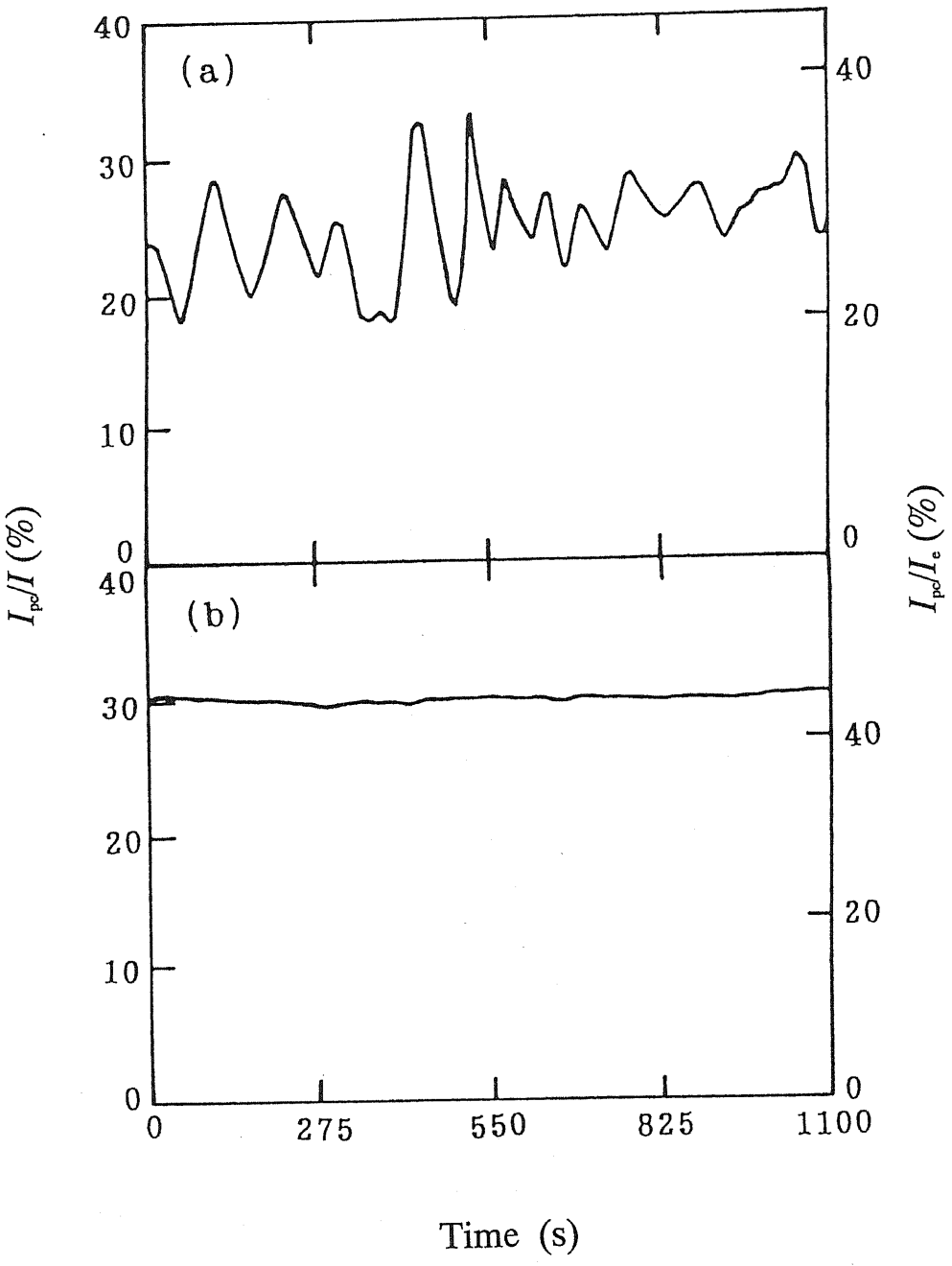

Fig. 2.9. Stability observations of the SPPCM for (a) Φ = 26° and (b) Φ = 35° polarization angles of the incident light under the same incident conditions as those of Fig. 2.4. The left ordinate corresponds to the I_{pc}/I percentage, and the right ordinate corresponds to the I_{pc}/I_e percentage.

2.5 Summary

In conclusion, a theory of two-wave mixing has been described, which was used to explain the self-generated fanning effect in photorefractive crystal SPPCM. The dynamic instability of the SPPCM is further investigated. The dynamic instability of the SPPCM originating from the competition between the self-generated fanning effect and the SPPCM formation has been analyzed and proved in theory and experiment. The self-generated fanning effect inside a photorefractive crystal can be effectively decreased by the ordinary-polarized component of the partially extraordinary-polarized light. The dynamic instability can be eliminated by restraining self-generated fanning. Whenever the extraordinary-polarized light does not correspond to the stable operation in the SPPCM, a partially extraordinary-polarized light beam is able to yield stable operation of the SPPCM. We believe that these results may also be realized in other photorefractive crystal SPPCMs because the self-generated fanning effect exists in other photorefractive crystals such as $BaTiO_3$ and $SrBaNb_2O_6$.

References

1. J. Feinberg, *Opt. Lett.* **7**, 486 (1982).
2. P. Gunter and J. P. Huignard, *Photorefractive Materials and Their Application II,* Springer-Verlag, (1989).
3. J. Feinberg, *Opt. Lett.* **8,** 569 (1983).
4. A. M. C. Smout, R. W. Eason, and M. C. Gower, *Opt. Commun.* **59,** 77 (1986).
5. J. Gauthier, P. Narum, and R. W. Boyd, *Phys. Rev. Lett.* **58,** 1640 (1987).
6. A. V. Nowak, T. R. Morre, and R. A. Fisher, *J. Opt. Soc. Am.* B **5,** 1864 (1988).
7. T. Rauch, C. Denz, and T. Tschudi, *Opt. Commun.* **88,** 160 (1992).
8. P. M. Jeffrey and R. W. Eason, *J. Opt. Soc. Am.* B **11,** 476 (1994).
9. P. Gunter, E. Voit, M. Z. Zha, and J. Albers, *Opt. Commun.* **55,** 210 (1985).
10. M. C. Gower and P. Hribek, *J. Opt. Soc. Am.* B **5,** 1750 (1988).
11. A. K. Majumdar and J. L. Kobesky, *Opt. Commun.* **75,** 339 (1990).
12. X. Gao, *Doctor Thesis, Grad. School of Electron. Sci. Technol. Shizuoka University,* (1995).
13. Y. Zheng, A. Sasaki, X. Gao, and H. Aoyama, *Opt. Lett.* **20,** 267 (1995).
14. A. M. Glass, *Opt. Eng.* **17,** 470 (1978).
15. D. Z. Anderson and J. Feinberg, *IEEE J. Quantum Electron.* **25,** 635 (1989).
16. M. Horowitz, D. Kligler, and B. Fischer, *J. Opt. Soc. Am.* B **8,** 2204 (1991).
17. M. Horowitz, R. Daisy, and B. Fischer, *J. Opt. Soc. Am.* B **9,** 1685 (1992).
18. J. Feinberg, D. Heiman, A. R. Tanguay, Jr., and R. W. Hellwarth, *J. Appl. Phys.* **51,** 1297 (1980); **52,** 537 (1981).
19. K. R. MacDonald and J. Feinberg, *J. Opt. Soc. Am.* **73,** 5488 (1983).
20. D. Sun, J. Chen, X. Lu, Y. Song, Z. Shao, and H. Chen, *J. Appl. Phys.* **70,** 33

(1991).

21. N. V. Bogodaev, L. I. Ivleva, A. S. Korshunov, A. V. Mamaev, N. N. Polozkov, and A. A. Zozulya, *J. Opt. Soc. Am.* B **10,** 1054 (1993).
22. A. A. Zozulya, *IEEE J. Quantum Electron.* **29,** 538 (1993).
23. S. Orlov, M. Segev, A. Yariv, and G. C. Valley, *Opt. Lett.* **19,** 578 (1994).

Chapter 3

High-Performance Double Phase-Conjugate Mirror (DPCM) in Cu:KNSBN Crystal

How to form a high-performance double phase-conjugate mirror in a Cu:KNSBN crystal is demonstrated. A theory of four-wave mixing in a double phase-conjugate mirror is described. Based on great diffraction efficiency of four-wave mixing and low light losses, a high-performance Cu:KNSBN double phase-conjugate mirror is formed with modified-bridge geometry. A phase-conjugate transmissivity as high as 63% with 97% relative stability is observed, using a low power argon-ion laser of 514.5 nm wavelength in Brewster angle incidence.

3.1 Introduction

The double phase-conjugate mirrors (DPCMs) generates the phase-conjugate light beam of each of two incident light beams, which is one of the most popular four-wave mixing (FWM) geometries for the conjugation of two light beams in a photorefractive medium. The two incident beams need not be coherent with each

other. The DPCMs have drawn great attention because of their wide applications in, for example, optical image processing, optical communication and adaptive optical interconnection.[1-12] In photorefractive crystals, the different geometrical DPCMs have been formed, such as the double phase-conjugate mirror (DPCM), the mutually incoherent beam coupler, the bird-wing DPCM, the frog-legs DPCM, the bridge DPCM, and the modified-bridge DPCM [these DPCMs are shown in Figs. 3.1(a) ~ 3.1(f)].[2,13-20] However, the efficiency of DPCMs was not too high. Here, the efficiency of the DPCM is defined as the ratio of the total phase-conjugate output intensity and the total incident light intensity, which is equal to the phase-conjugate transmissivity. In general, the phase-conjugate transmissivity of these DPCMs is not over 35%.[2,13-18,21-23] The performance enhancement of the DPCM has been required for its applications. Recently, a stable high-efficiency DPCM in a Cu:KNSBN crystal was first reported by Gao *et al.*[24] However, how to form a high-performance DPCM in a photorefractive crystal has not been revealed yet.

In this chapter, a theory of four-wave mixing in a DPCM is described. How to form a high-performance DPCM in a photorefractive Cu:KNSBN crystal is demonstrated.[25] For the formation of a high-efficiency DPCM, we give what aspects should be considered. Based on the theoretical analysis, a high-performance DPCM with a very high phase-conjugate transmissivity is formed under Brewster angle incidence.

3.2 Four-Wave Mixing in a DPCM

Here we present a one-dimensional coupled-plane-wave theory of four-wave mixing for a DPCM. Although the interaction of four-wave mixing is two dimensional, two-dimensional coupled-wave theory is too complex to use.[26-28] The

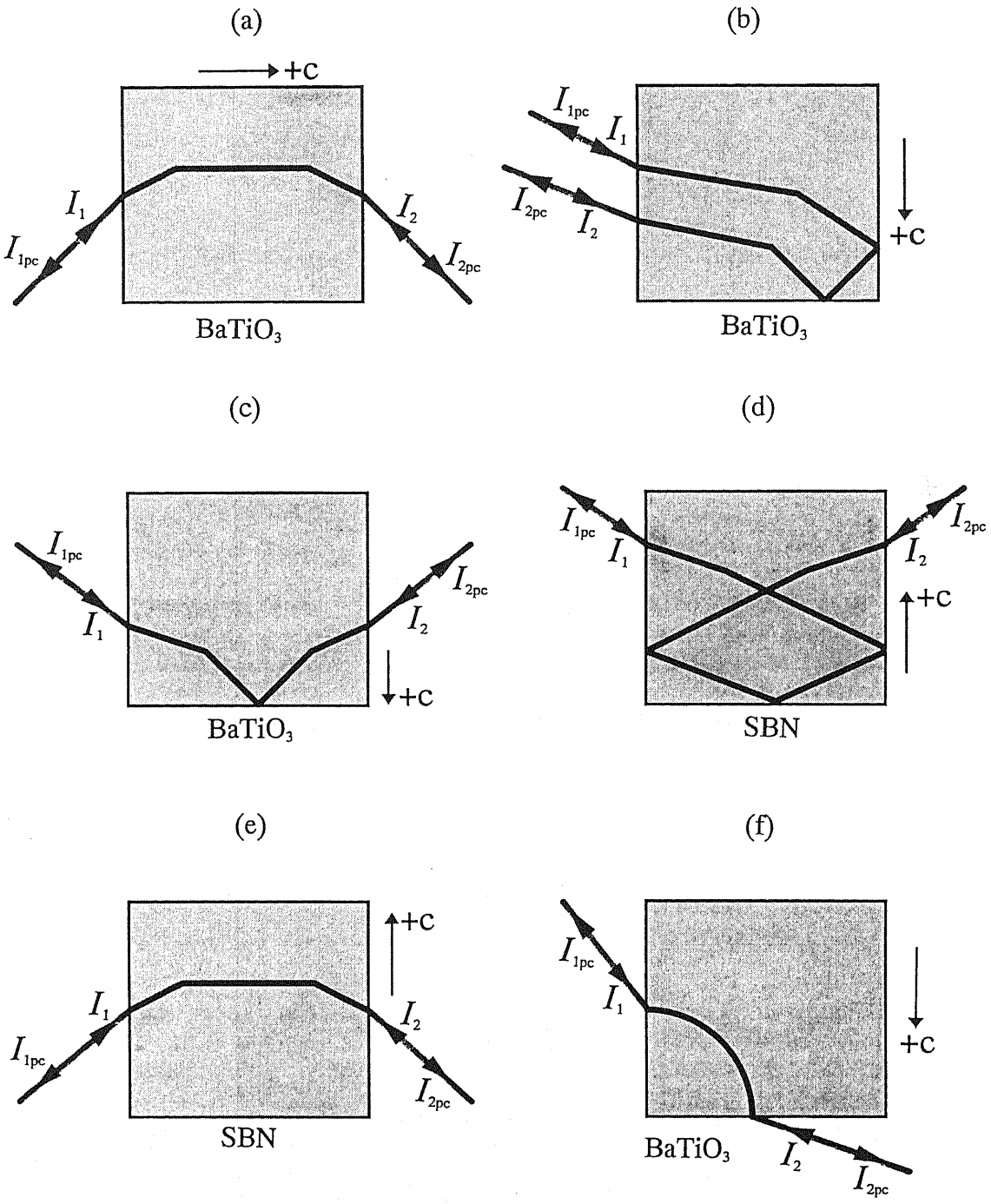

Fig. 3.1. Drawings of different geometrical DPCMs. (a) Double phase-conjugate mirror. (b) Mutually incoherent beam coupler. (c) Bird-wing DPCM. (d) Frog-legs DPCM. (e) Bridge DPCM. (f) Modified-bridge DPCM.

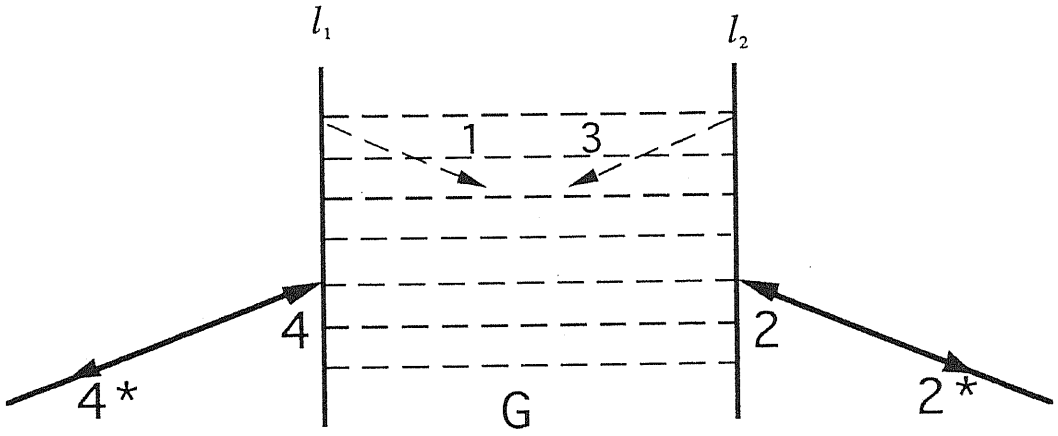

Fig. 3.2. Simplified diagram of four-wave mixing in a DPCM.

simple one-dimensional coupled-plane-wave theory is widely accepted as an effective tool to explain quantitatively and qualitatively the four-wave mixing in phase-conjugate mirror. Thus, we use the conventional and effective one-dimensional coupled-plane-wave theory to explain qualitatively the performance of DPCM with one interaction region. While in principle this theory can be extended to the any geometrical DPCMs with two interaction regions. One interaction region case is shown in Fig. 3.2. Beams 2 and 4 are incident upon a photorefractive crystal. The interaction region extends from $l_1 \le z \le l_2$. Beam 4 is deflected by grating G into beam 1, which is phase conjugate to beam 2. Similarly, beam 2 is deflected by grating G into beam 3, which is phase conjugate to beam 4. If the jth beam has an optical electric field

$$E_j = A_j \exp[i(\boldsymbol{k}_j \cdot \boldsymbol{r} - \omega t)]. \tag{3.1}$$

According to the wave equation and using the slowly varying amplitudes approximation, the four-wave mixing equations in the interaction region with the transmission grating are given by (neglecting absorption) [1,29,30]

$$\frac{dA_1}{dz} = \frac{\gamma g}{I_0} A_4, \tag{3.2}$$

$$\frac{dA_4^*}{dz} = \frac{-\gamma g}{I_0} A_1^*, \tag{3.3}$$

$$\frac{dA_3}{dz} = \frac{-\gamma g}{I_0} A_2, \tag{3.4}$$

$$\frac{dA_2^*}{dz} = \frac{\gamma g}{I_0} A_3^*, \tag{3.5}$$

where γ is the coupling coefficient given by Eq. (2.5) in chapter 2, I_0 is the total intensity, i.e.,

$$I_0 = |A_1|^2 + |A_2|^2 + |A_3|^2 + |A_4|^2, \tag{3.6}$$

and the quantity g is defined as

$$g = A_1 A_4^* + A_2^* A_3. \tag{3.7}$$

The boundary conditions are

$$A_1(l_1) = 0, \tag{3.8}$$

$$A_3(l_2) = 0. \tag{3.9}$$

According to energy conservation the following quantities are constant:

$$d_1 = |A_1|^2 + |A_4|^2 = I_1 + I_4 = I_4(l_1), \tag{3.10}$$

$$d_2 = |A_2|^2 + |A_3|^2 = I_2 + I_3 = I_2(l_2), \tag{3.11}$$

$$c = A_1 A_2 + A_3 A_4. \tag{3.12}$$

In terms of the conserved quantities, the phase conjugate reflectivities R_1 and R_2 can be expressed as

$$R_1 = \left|\frac{A_3(l_1)}{A_4^*(l_1)}\right|^2 = \left|\frac{c}{d_1}\right|^2, \tag{3.13}$$

$$R_2 = \left|\frac{A_1(l_2)}{A_2^*(l_2)}\right|^2 = \left|\frac{c}{d_2}\right|^2, \tag{3.14}$$

and using the conservation constant c of Eq. (3.12), where $c(l_1) = c(l_2)$, in conjunction with the boundary conditions of Eqs. (3.8) and (3.9), leads to

$$\frac{A_1(l_2)}{A_4(l_1)} = \frac{A_3(l_1)}{A_2(l_2)}. \tag{3.15}$$

Thus the transmissivities T and T' of the two incident beams through the interaction region are equal. The transmissivity, that is, the diffraction efficiency η of four-wave mixing, is given by

$$\eta = T = \left|\frac{A_1(l_2)}{A_4(l_1)}\right|^2 = T' = \left|\frac{A_3(l_1)}{A_2(l_2)}\right|^2 = \frac{|c|^2}{d_1 d_2}. \tag{3.16}$$

The only unknown quantity in Eq. (3.16) is the conservation constant c. Now we determine the conservation constant c. We define

$$\Delta = d_2 - d_1, \tag{3.17}$$

$$r = (\Delta^2 + 4|c|^2)^{1/2}, \tag{3.18}$$

and

$$\mu = \frac{\gamma r}{2I_0}. \tag{3.19}$$

Using Eqs. (3.10), (3.11), and (3.12), the coupled Eqs. (3.2), (3.3), (3.4), and (3.5) have the solution

$$\frac{A_1(z)}{A_2^*(z)} = \frac{2c\tanh[\mu(z-l_1)]}{\Delta\tanh[\mu(z-l_1)]+r}, \tag{3.20}$$

$$\frac{A_3(z)}{A_4^*(z)} = \frac{-2c\tanh[\mu(z-l_2)]}{\Delta\tanh[\mu(z-l_2)]+r}. \tag{3.21}$$

Evaluating Eqs. (3.20) and (3.21) at the boundaries $z = l_1$ and $z = l_2$ [see Eqs. (3.13) and (3.14)] yields

$$\tanh\left[\frac{\gamma(l_2-l_1)r}{2I_0}\right] = \frac{r}{I_0}. \tag{3.22}$$

The transcendental equation can be rewritten by substituting for r/I_0 in Eq. (3.22):

$$\tanh\left\{\frac{\gamma l\left[(d_2-d_1)^2+4|c|^2\right]^{1/2}}{2(d_2+d_1)}\right\} = \frac{\left[(d_2-d_1)^2+4|c|^2\right]^{1/2}}{d_2+d_1}, \tag{3.23}$$

where $l = l_2 - l_1$. According to Eqs. (3.16) and (3.23), we can solve the diffraction

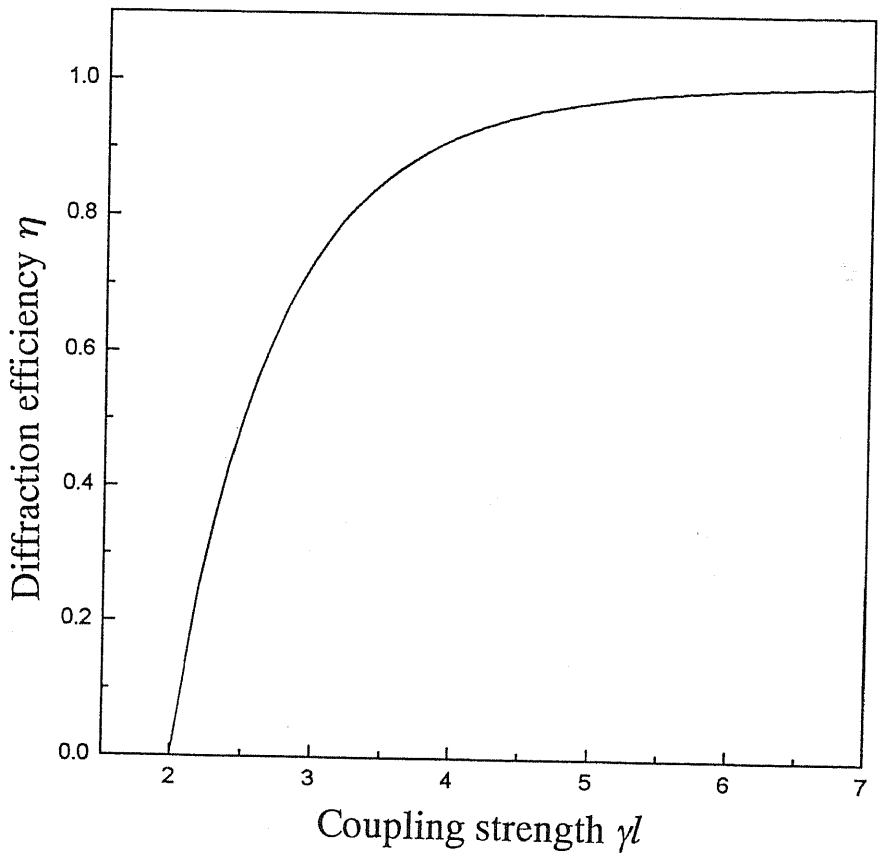

Fig. 3.3. Calculated diffraction efficiency η of four-wave mixing versus the coupling strength γl for the incident intensity normalization $I_2 + I_4 = 1$ and the ratio $q = I_2/I_4 = 1$.

efficiency of four-wave mixing in terms of the independent variables (the incident intensities d_1, d_2, and the coupling strength γl) by computer.

Figure 3.3 shows the calculated diffraction efficiency η of four-wave mixing as a function of coupling strength γl for the incident intensity normalization $I_2 + I_4 = 1$ and the ratio $q = I_2/I_4 = 1$. We find that the large coupling strength γl (the large coupling constant γ and the large interaction region l) corresponds to the high diffraction efficiency of four-wave mixing in the DPCM, when the coupling strength γl is above the threshold 2. In the DPCM, a high diffraction efficiency of four-wave mixing corresponds to a high phase-conjugate transmissivity (or the efficiency) of the DPCM. Thus, to achieved a high efficiency of the DPCM, the large coupling constant γ and the large interaction region l are required.

3.3 Formation of the High-Performance DPCM with the Modified-Bridge Geometry

DPCMs are the devices of four-wave mixing. The phase-conjugate transmissivity of a DPCM can be written

$$T_{pc} = \eta(1 - R_1)(1 - R_2)e^{-\alpha L}, \tag{3.24}$$

where η is the diffraction efficiency of four-wave mixing. α is the absorption coefficient. R_1 and R_2 are the specular reflectivities of two faces in a photorefractive crystal, respectively. L is the light path length inside the crystal. According to Eq. (3.24), to obtain a high-performance DPCM, the following aspects should be considered: first, in the chosen geometrical DPCM, there should be a great diffraction efficiency of four-wave mixing, which requires a great coupling constant

γ and a large interaction region, according to the theoretical analysis of above section. Second, in the chosen geometrical DPCM, the light losses should be small. The light losses include the absorption and scattering loss inside the crystal, and the specular reflection loss on the surfaces of the crystal. Third, a high efficiency will contribute to the stable operation of the DPCM.

In Cu:KNSBN crystal, there are two large electrooptic coefficients, r_{42} (400 pm/V) and r_{33} (270 pm/V).[31] Therefore, in Cu:KNSBN crystal, the modified-bridge DPCM, the bird-wing geometrical DPCM and the bridge DPCMs can be formed using mostly r_{42} and r_{33},[24,32,33] respectively. In the modified-bridge DPCM, there is a large interaction region, as shown in Fig. 3.4. Once the modified-bridge DPCM was formed, even if one incident light beam was obstructed, the corresponding phase-conjugate beam initially underwent no change and was still generated until the formed grating was erased. Thus, we consider that the modified-bridge DPCM is formed from the transmission grating of four-wave mixing. According to Eq. (2.5) described in chapter 2, we calculated the coupling coefficient γ as a function of the symmetrical incident angle $\Phi = \Phi_1 = \Phi_2$, under extraordinary-polarized light beam incidence in Cu:KNSBN crystal, as shown in curve 1 of Fig. 3.5. In our experimental condition, γ is large (γ = 2.3-2.5 mm^{-1}). In the interaction region, each incident light beam is diffracted two times on Bragg diffraction in two directions to form the phase-conjugate light beam of another incident light beam.[33] Along the diffraction directions of the large interaction region, the average interaction lengths l_1, l_2 and l_3 are long, as shown in Fig. 3.4. In the diffraction directions, the average coupling strengths γl_i (i = 1, 2 and 3) exceed 7, which are enough great values from Fig. 3.3. Therefore, we consider that, in the interaction region, the diffraction efficiency of the four-wave mixing is great enough to get a high efficiency in modified-bridge DPCM. However, in bridge geometrical DPCM of the Cu:KNSBN crystal, the

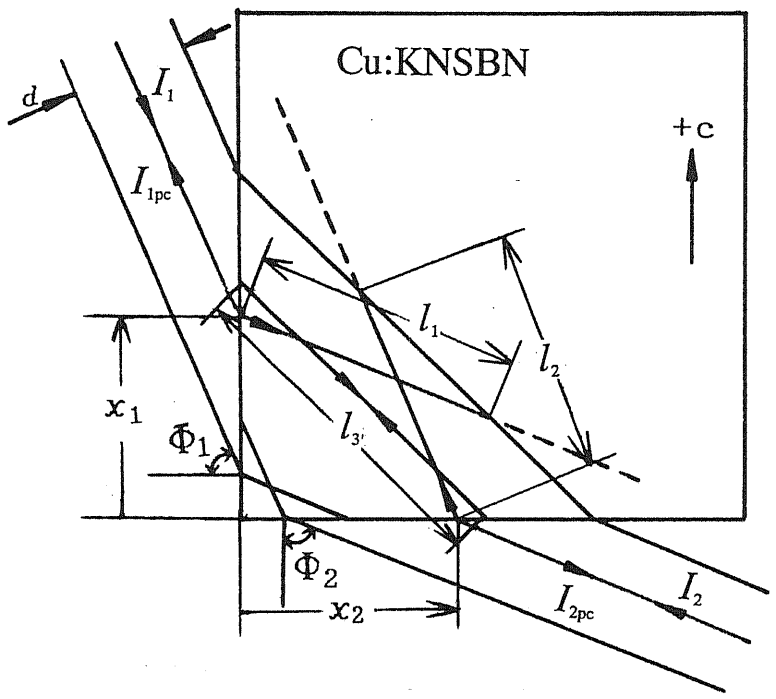

Fig. 3.4. Schematic of the modified-bridge DPCM in a Cu:KNSBN crystal. The Cu:KNSBN crystal is 6 mm × 6 mm × 6 mm ($a \times b \times c$). Incident beam diameter d is 1.6 mm.

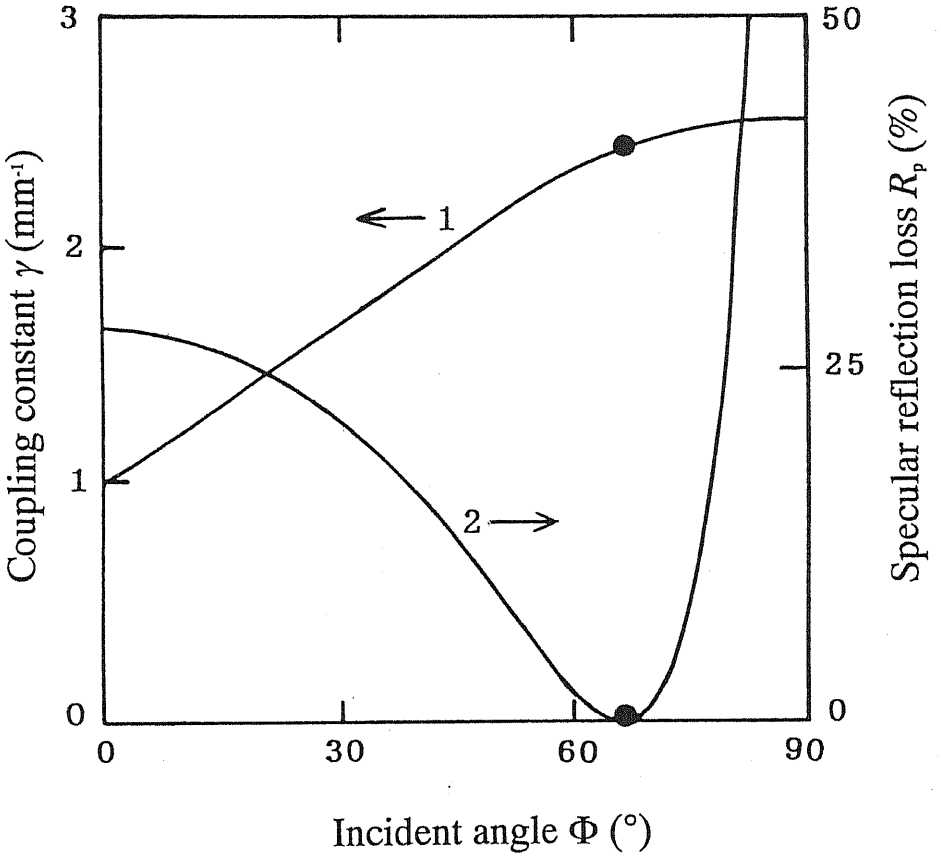

Fig. 3.5. Curve 1 is the calculated coupling constant γ as a function of the symmetrical incident angle $\Phi = \Phi_1 = \Phi_2$ in the modified-bridge DPCM, based on the following values: λ = 514.5 nm, $N \sim 5 \times 10^{16}$, ε_{11} = 588, ε_{33} = 500, n_o = 2.30, n_e = 2.27, r_{13} = 50 pm/V, r_{42} = 400 pm/V, r_{33} = 270 pm/V. Curve 2 is the calculated specular reflection loss R_p on the two surfaces of the crystal as a function of the symmetrical incident angle $\Phi = \Phi_1 = \Phi_2$. The closed circles correspond to the incident angle Φ = 67°.

calculated coupling coefficient is small (γ = 1.1-1.3 mm^{-1}). Although the bird-wing DPCM of the Cu:KNSBN crystal has the same coupling constant value as the modified-bridge DPCM, the diffraction efficiency is small, because its two separated interaction regions are small. When the diffraction efficiency of the four-wave mixing is high enough to obtain a high efficiency, attention should be paid to the decrease of the light losses including the absorption and scattering loss inside the crystal, and the specular reflection loss on the surfaces of the crystal in the DPCM. The measured exponential coefficient of the absorption is 0.78 cm^{-1}, which leads to a large loss of the light intensity in the used Cu:KNSBN crystal. The light path length L of the modified-bridge DPCM is only half that of the bridge DPCM and the bird-wing DPCM. Thus the absorption and scattering loss of the modified-bridge DPCM is much smaller than that of other DPCMs. Therefore, in the modified-bridge DPCM, the efficiency is much enhanced.

In another aspect, since the Cu:KNSBN crystal has large refractive indexes (n_e = 2.27, n_o = 2.30),[24] the specular reflection loss cannot be neglected. When the light beam is vertically incident on the crystal, the light loss of two faces in the crystal is as high as 28% for extraordinary-polarized light case. Based on the Fresnel reflection formula, the amplitude reflectivity is given by

$$r_e = \frac{\tan(\Phi_1 - \Phi_{1t})}{\tan(\Phi_1 + \Phi_{1t})}, \tag{3.25}$$

where Φ_{1t} is the refraction angle. It is written by the law of refraction

$$n_{1e} \sin\Phi_1 = n_e \sin\Phi_{1t}, \tag{3.26}$$

where n_{1e} = 1. Then the specular reflectivity is given by

$$R_e = |r_e|^2 = \left|\frac{\tan(\Phi_1 - \Phi_{1t})}{\tan(\Phi_1 + \Phi_{1t})}\right|^2 . \qquad (3.27)$$

It is just the specular reflection loss of one surface in the DPCM. The specular reflection loss is a function of the incident angle. The calculated specular reflection loss of two surfaces as a function of the symmetrical incident angle $\Phi = \Phi_1 = \Phi_2$ is shown in curve 2 of Fig. 3.5, when the extraordinary-polarized light is incident upon the Cu:KNSBN crystal. In the modified-bridge DPCM, the optimum incident angle with a great coupling constant is about 67°, which is just in Brewster angle range. In this incident angle range, the specular reflection of the crystal surface is minimum, and the specular reflection loss is effectively diminished. Therefore, the efficiency of the DPCM is enhanced. From Fig. 3.5, we can see that when the incident angle is in the Brewster angle range, the coupling coefficient γ is also located in a large value range. In this case, the Cu:KNSBN modified-bridge DPCM has a large diffraction efficiency of four-wave mixing, and its light loss is small. Therefore, it is possible that the Cu:KNSBN modified-bridge DPCM reaches a very high efficiency in Brewster angle incident.

Based on the above considerations, we made the experiments of the modified-bridge DPCM in a Cu:KNSBN crystal, using a low power argon-ion laser of λ = 514.5 nm, under Brewster angle incidence. Figure 3.6 shows the measured phase-conjugate transmissivity T_{pc} ($T_{pc} = I_{2pc}/I_1 \approx I_{1pc}/I_2$) with different incident location x_2 at the certain incident position x_1. The maximum phase-conjugate transmissivity reaches 63%, which is the highest value in the reported DPCMs to our knowledge. In our experimental, the two phase-conjugate transmissivities are approximately identical. In the most suitable incident positions (x_1, x_2 = 2 ~ 2.5 mm), the light path

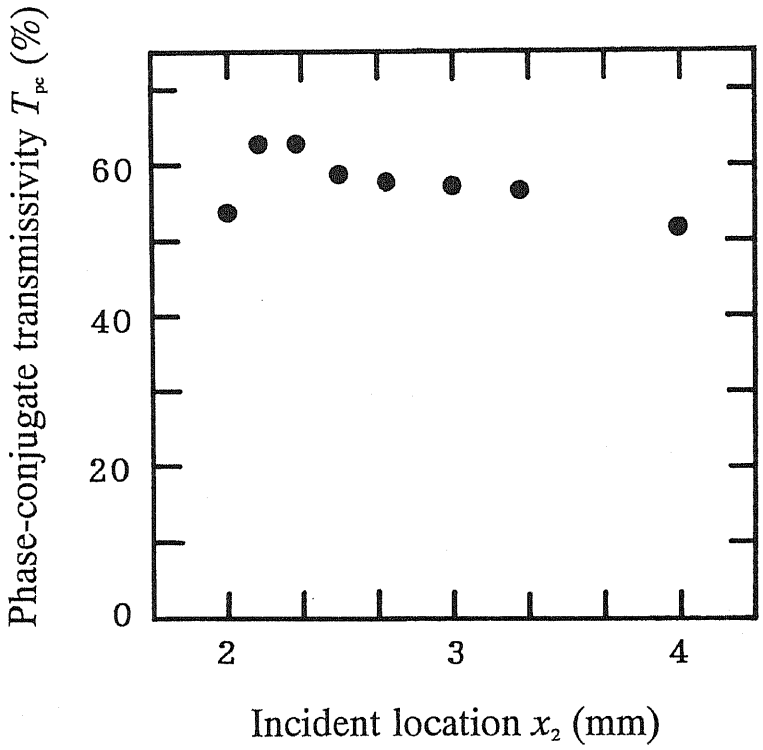

Fig. 3.6. Phase-conjugate transmissivity T_{pc} ($T_{pc} = I_{2pc}/I_1 \approx I_{1pc}/I_2$) versus incident position x_2, at the incident position x_1 = 2.2 mm, the symmetrical incident angle $\Phi = \Phi_1 = \Phi_2 = 67°$ and the incident power $I = I_1 = I_2 = 4$ mW.

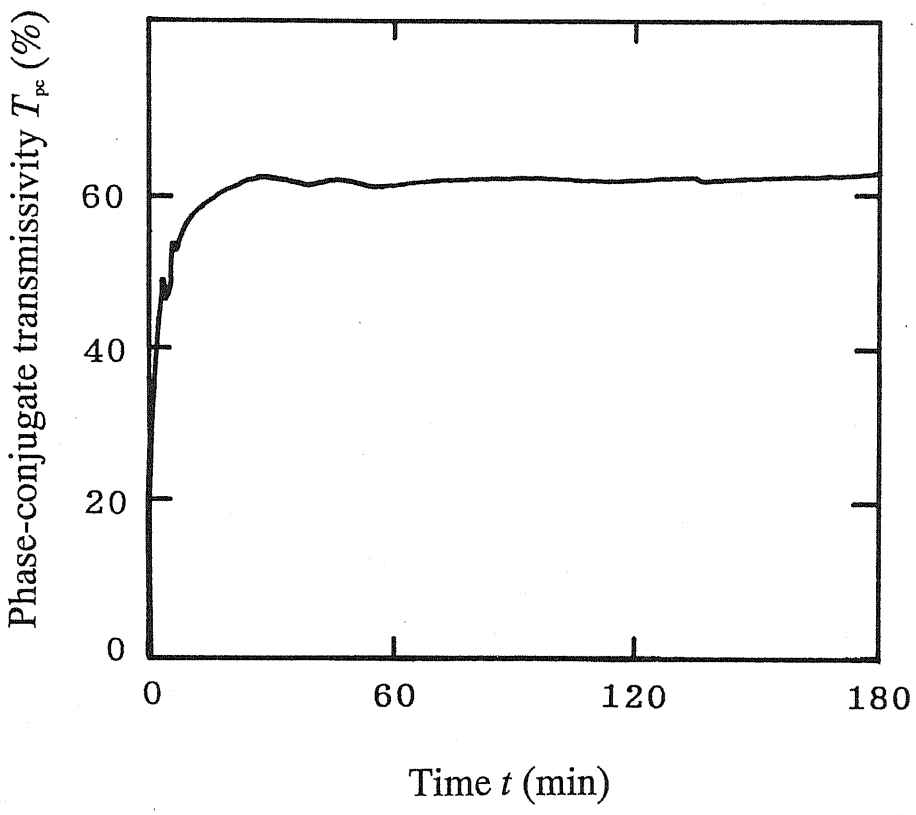

Fig. 3.7. Observation on the stability of the phase-conjugate transmissivity in x_2 = 2.3 mm, when the incident conditions are the same as those in Fig. 3.6.

inside the crystal is small, thus the absorption and scattering loss is small. Therefore, in this case, the phase-conjugate transmissivity has maximum value.

Also, the high efficiency results in a very stable operation of the modified-bridge DPCM. Figure 3.7 is an observation of stability of the modified-bridge DPCM over a long period of time. The relative stability is as high as 97% which is a very high value in a long-time observation in comparison with other DPCMs. The high efficiency decreases the turbid fanning inside the crystal and the disturbance of the turbid fanning to the grating of the DPCM.

3.4 Summary

In conclusion, a plan-wave theory of four-wave mixing has been given. How to form a high-performance DPCM in a Cu:KNSBN crystal has been described. Based on the great diffraction efficiency of four-wave mixing, the low light losses including absorption and scattering loss inside the crystal, and specular reflection loss on the surfaces of the crystal, a high-performance modified-bridge DPCM has been formed in a Cu:KNSBN crystal. A phase-conjugate transmissivity of as high as 63% with 97% relative stability was observed in Brewster angle incidence. The efficiency of the modified-bridge DPCM is the highest value in reported DPCMs to our knowledge.

References

1. B. Fischer, S. Sternklar, and S. Weiss, *IEEE J. Quantum Electron.* **QE-25,** 550 (1989).
2. S. Sternklar, S. Weiss, and B. Fischer, *Opt. Eng.* **26,** 423 (1987).
3. R. J. Anderson, E. J. Sharp, G. L. Wood, and G. J. Salamo, *Appl. Opt.* **35,** 854 (1996).
4. J. M. Yarrison-Rice, E. J. Sharp, G. L. Wood, and R. R. Neurgaonkar, *Appl. Opt.* **35,** 1904 (1996).
5. J. Shamir, H. J. Caulfield, and B. M. Hendrickson, *Appl. Opt.* **27,** 2912 (1988).
6. Q. C. He, J. Shamir, and J. G. Duthie, *Appl. Opt.* **28,** 306 (1989).
7. S. Weiss, M. Segev, S. Sternklar, and B. Fischer, *Appl. Opt.* **27,** 3422 (1988).
8. M. P. Schamschula and H. J. Caulfield, *Opt. Lett.* **16,** 1421 (1991).
9. A. Chiou, P. Yeh, C. Yang, and C. Gu, *Opt. Lett.* **20,** 1125 (1995).
10. C. Medrano, M. Zgonik, P. Bernasconi, and P. Gunter, *Opt. Commun.* **128,** 177 (1996).
11. Y. Zheng, A. Sasaki, and X. Gao, *Opt. Commun.* **136,** 437 (1997).
12. Y. Zheng and A. Sasaki, *Jpn. J. Appl. Phys.* **36,** L676 (1997).
13. S. Weiss, S. Sternklar, and B. Fischer, *Opt. Lett.* **12,** 114 (1987).
14. S. Sternklar, S. Weiss, and B. Fischer, *Appl. Opt.* **25,** 4518 (1986).
15. R. W. Eason and A. M. C. Smout, *Opt. Lett.* **12,** 51 (1987).
16. A. M. C. Smout and R. W. Eason, *Opt. Lett.* **12,** 498 (1987).
17. M. D. Ewbank, *Opt. Lett.* **13,** 47 (1988).
18. M. D. Ewbank, R. A. Vazquez, R. R. Neurgaonkar, and J. Feinberg, *J. Opt. Soc. Am.* B **7,** 2306 (1990).
19. E. J. Sharp, W. W. Clark III, M. J. Miller, G. L. Wood, B. Monson, G. J. Salamo,

and R. R. Neurgaonkar, *Appl. Opt,* **29,** 743 (1990).

20. D. Wang, Z. Zhang, Y. Zhu, S. Zhang, and P. Ye, *Opt. Commun.* **73,** 495 (1989).
21. C. Wu and Y. Zhao, *Opt. Lett.* **18,** 98 (1993).
22. Z. Zhang, Y. Zhu, C. Yang, and P. Fu, *J. Appl. Phys.* **74,** 2137 (1993).
23. G. W. Ross and R. W. Eason, *Opt. Lett.* **18,** 571 (1993).
24. X. Gao, A. Sasaki, and Y. Zheng, *Jpn. J. Appl. Phys.* **32,** L1654 (1993).
25. Y. Zheng, A. Sasaki, X. Gao, and H. Aoyama, *Opt. Commun.* **116,** 449 (1995).
26. V. V. Eliseev, V. T. Tikhonchuk, and A. A. Zozulya, *J. Opt. Soc. Am.* B **8,** 2497 (1991).
27. K. D. Shaw, *Opt. Commun.* **90,** 133 (1992).
28. K. D. Shaw, *Opt. Commun.* **103,** 326 (1993).
29. B. Fischer, M. Cronin-Golomb, J. O. White, and A. Yariv, *Opt. Lett.* **6,** 519 (1981).
30. K. R. MacDonald and J. Feinberg, *J. Opt. Soc. Am.* **73,** 548 (1983).
31. X. Yue, X. Lu, Y. Song, Z. Shao, D. Sun, Q. Jian, and H. Chen, *Appl. Phys.* B **53,** 319 (1991).
32. Y. Zheng, A. Sasaki, and X. Gao, *Nonlinear Opt.* **8,** 115 (1994).
33. Y. Zheng, A. Sasaki, X. Gao, H. Aoyama, and J. Fukaya, *Jpn. J. Appl. Phys.* **34,** 5405 (1995).

Chapter 4

High-Efficiency Bridge Double Phase-Conjugate Mirrors (DPCMs) in Cu:KNSBN Crystals

The formation of high-efficiency double phase-conjugate mirrors with the bridge incident geometry is demonstrate in Cu:KNSBN crystals. These bridge double phase-conjugate mirrors have high efficiency, even under low incident power. For crystals with different absorption coefficients, the optimum incident geometries of the bridge double phase-conjugate mirrors are observed and discussed.

4.1 Introduction

The double phase-conjugate mirror (DPCM) was reported by Weiss *et al.* in 1987, since then, DPCMs have drawn great interest for their wide applications. In some photorefractive crystals, different geometrical DPCMs have been reported, as shown in Figs. 3.1(a) ~ 3.1(f). In these DPCMs, the phase-conjugate transmissivity was not too high. In chapter 3, based on the great diffraction efficiency of four-wave mixing, the low light losses including absorption and scattering loss inside the

crystal, and specular reflection loss on the surfaces of the crystal, a high-performance modified-bridge DPCM in a Cu:KNSBN crystal was formed. However, in some applications, for example a three-dimensional object projection in next chapter, the bridge geometry of DPCM is needed. Previously, the bridge DPCM was observed only in $BaTiO_3$ and $SrBaNb_2O_6$ crystals.[1,2] Although $BaTiO_3$ crystal has a very large electrooptic coefficient (r_{42}), it suffers from an inconvenient Curie temperature. In recent, we formed the bridge DPCMs, the modified-bridge DPCM and the bird-wing DPCM,[3-6] by using Cu:KNSBN crystals having the advantage of convenient usability.[7] In this chapter, we describe the formation of bridge DPCMs in Cu:KNSBN crystals using a low-power (milliwatt order) argon laser (λ = 514.5 nm). Two kinds of high-efficiency bridge DPCMs are formed. For the crystals with different absorption coefficients, the optimum incident geometries are explored. The experimental results show also that the high-efficiency DPCMs are very suitable for work at low incident powers.

4.2 Formation of the High-Efficiency Bridge DPCMs in Cu: KNSBN Crystals with Different Absorption Coefficients

The experimental arrangement is shown in Fig. 4.1, where two extraordinary polarized light beams 1 (with intensity I_1) and 2 (with intensity I_2) of the laser (514.5 nm wavelength) are incident on opposite faces of a Cu-doped KNSBN (0.01-0.06 wt % doped CuO) crystal, which has been called the bridge geometry of DPCM by Sharp *et al.*[1] The incident light beam diameter is 1.6 mm. The path difference of the two incident light beams is 50 cm, which is much longer than the coherence length (5 cm) of the laser. Therefore, the two light beams are mutually incoherent. Beams 1* (with intensity I_{1pc}) and 2* (with intensity I_{2pc}) are the phase-conjugate beams

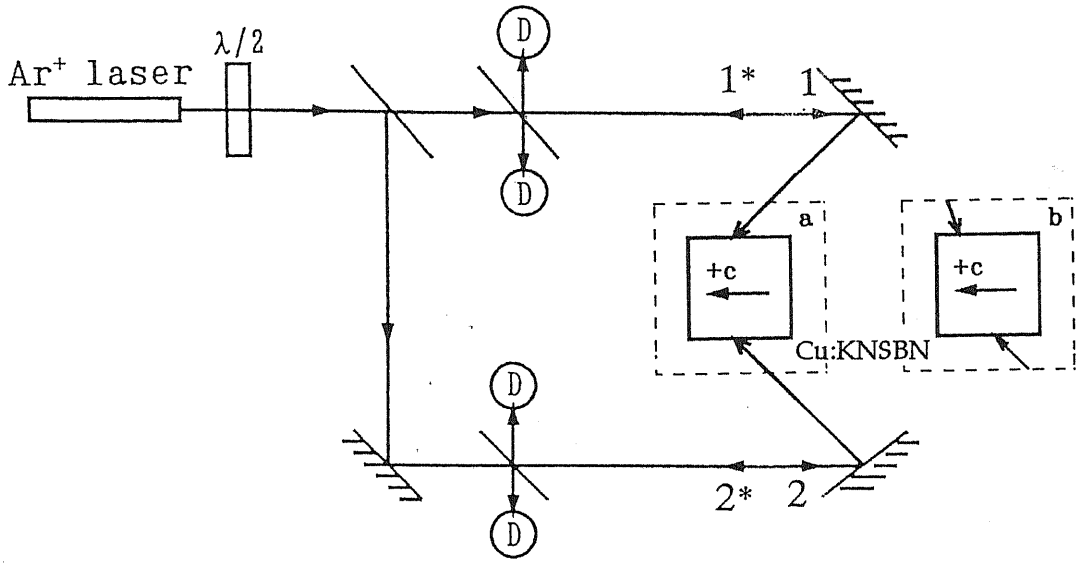

Fig. 4.1. Experimental arrangement of the Cu:KNSBN bridge DPCMs. (a) Symmetrical-bridge geometry. Here the incident angles and the positions of two incident beams are symmetrical. (b) Asymmetrical-bridge geometry. Here the incident angles and the positions of two incident beams are asymmetrical.

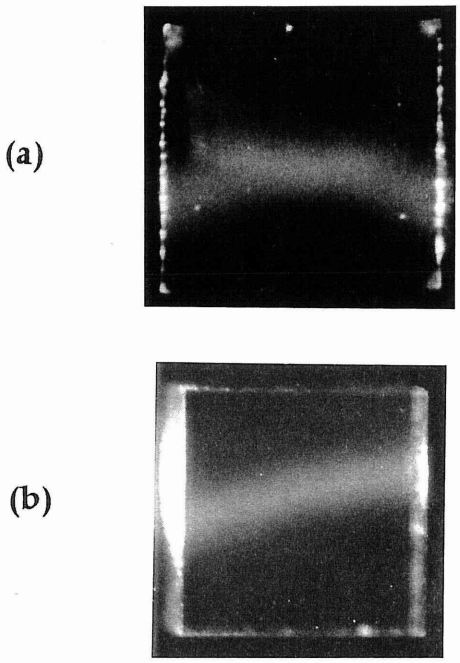

Fig. 4.2. Photographs of the formed Cu:KNSBN bridge DPCMs. (a) Symmetrical-bridge geometry. (b) Asymmetrical-bridge geometry.

generated by the bridge DPCMs. In our experiments, two bridge incident geometries were adopted, as shown in Fig. 4.1. In the incident geometry shown in Fig. 4.1(a), the incident angles and the positions of two incident light beams are symmetrical. This is called the symmetrical-bridge geometry of DPCM. In the incident geometry shown in Fig. 4.1(b), the two incident angles and positions are asymmetrical, and this is called the asymmetrical-bridge geometry of DPCM. Two Cu:KNSBN crystals of about 6 mm × 6 mm × 6 mm were used. The two crystals have apparently different dopant concentrations. The exponential absorption coefficient of one crystal (crystal 1) is 0.78/cm, that of the other crystal (crystal 2) is 0.27/cm. Figures 4.2(a) and 4.2(b) show photographs of the Cu:KNSBN bridge DPCMs with the incident geometries shown in Figs. 4.1(a) and 4.1(b). After the bridge DPCMs were formed, if one input light beam was obstructed, the corresponding phase-conjugate light initially underwent no change and was still generated until the formed grating was erased. Therefore, the Cu:KNSBN bridge DPCM is also formed from the transmission grating of four-wave mixing.

4.3 Observation and Discussion of the Optimum Incident Geometries of DPCMs

The interaction regions of the symmetrical and asymmetrical bridge geometries of the DPCMs are shown in Figs. 4.3(a) and 4.3(b). In the two Cu:KNSBN bridge DPCMs, large interaction regions A_1 and A_2 are generated, respectively. According to the discussion of above chapter, the long interaction regions correspond to high diffraction efficiency of four-wave mixing. The interaction regions have two-dimensional distributions. The incident conditions, such as the incident beam diameter, the incident angle, the incident position, determine the interaction region

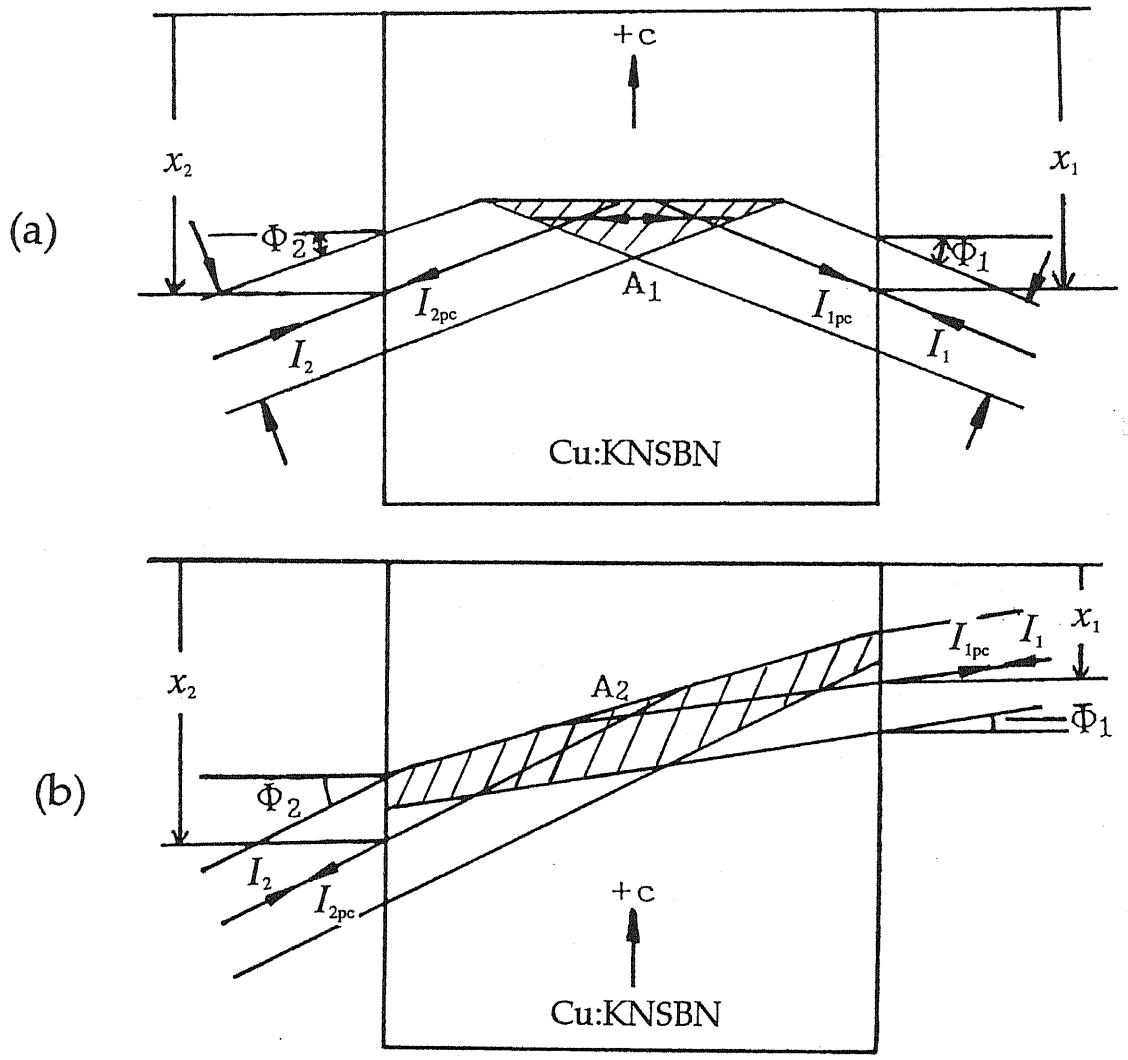

Fig. 4.3.. Schematics of the interaction regions in the Cu:KNSBN bridge DPCMs. Φ_1, Φ_2, incident angles; x_1, x_2, incident positions. (a) Symmetrical-bridge geometry. A_1, interaction region of the symmetrical-bridge DPCM. (b) Asymmetrical-bridge geometry. A_2, interaction region of the asymmetrical-bridge DPCM.

and therefore the efficiency of the DPCMs. However, inside the crystal a beam diameter that is too large leads to a pronounced self-generated fanning effect, which will result in low efficiency because self-generated fanning disturbs the DPCM grating and shares much of the incident light beams. Moreover, when the beam diameter inside the crystal is too large, the SPPCM and the bridge DPCM are easily generated simultaneously in the crystal. In this case, the phase-conjugate light output is very unstable because of the grating competition between the DPCM and the SPPCM.[8] When the incident beam diameter is certain, the incident geometry decides the beam diameter inside the crystal. For a different crystal a suitable incident geometry is need.

Figure 4.4 shows the phase-conjugate transmissivity T_{pc} ($T_{pc} = I_{2pc}/I_1 = I_{1pc}/I_2$) of the DPCMs using crystal 1 (circles) and crystal 2 (squares) with the symmetrical-bridge geometry shown in Fig. 4.1(a) versus the symmetric incident angle Φ ($\Phi = \Phi_1 = \Phi_2$). The experimental results show that the symmetrical-bridge DPCM with crystal 1 having a large absorption coefficient has high phase-conjugate transmissivity, and for the wide range of angles from 33° to 50°, the phase-conjugate transmissivities exceed 40%. The maximum phase-conjugate transmissivity is 45%. At the typical incident light intensity of $I = I_1 = I_2 = 2$ mW, the response time of the symmetrical-bridge DPCM with crystal 1 is 44 s for incident angle $\Phi = \Phi_1 = \Phi_2 =$ 47° and incident position $x = x_1 = x_2 = 3.5$ mm. However, in the symmetrical-bridge DPCM with crystal 2 having a small absorption coefficient, the response angle is small and the range of response angles is narrow. Moreover, its maximum phase-conjugate transmissivity is smaller than that of DPCM with crystal 1. Thus we can conclude that the DPCMs, which are formed by crystals having different absorption coefficients, correspond to different incident angles and different angle ranges. The DPCM having a small absorption coefficient corresponds to a small incident angle

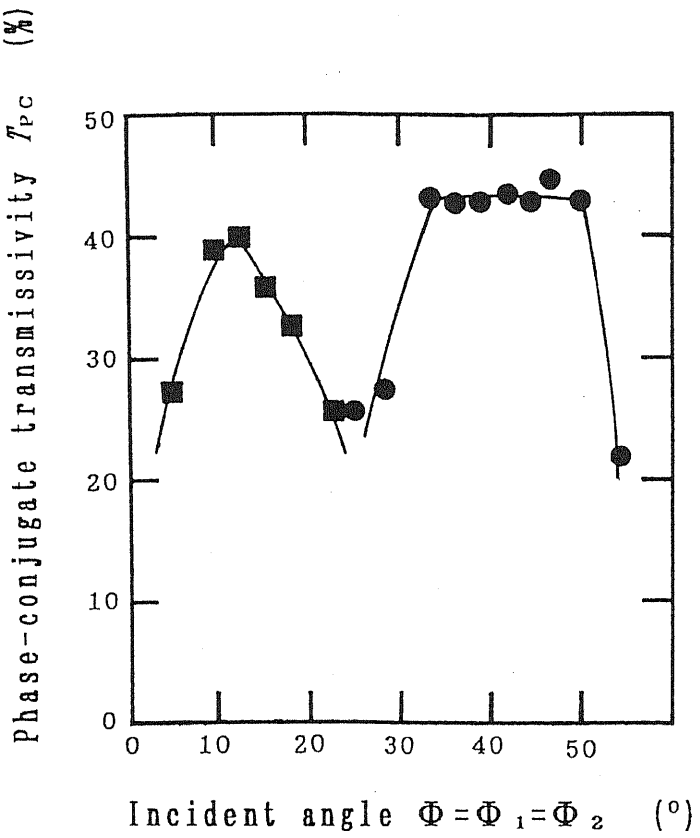

Fig. 4.4. Phase-conjugate transmissivity T_{pc} ($T_{pc} = I_{2pc}/I_1 = I_{1pc}/I_2$) versus the incident angle $\Phi = \Phi_1 = \Phi_2$ in symmetrical bridge geometry. Here the incident position is $x = x_1 = x_2 = 3.5$ mm and the incident light diameter is $d = 1.6$ mm. Circles show experimental results using crystal 1. Squares show the experimental results using crystal 2.

and a narrow angle range.

Although in symmetrical-bridge geometry, the efficiency of the DPCM with crystal 2 is smaller than that of DPCM with crystal 1, in asymmetrical-bridge incident geometry, we have observed the opposite result. Under the optimum incident conditions (Φ_1 = 21°, Φ_2 = 41°, and x_1 = 2 mm, x_2 = 3.3 mm) of asymmetrical-bridge geometry, the phase-conjugate transmissivity of the DPCM with crystal 2 reaches 50%. However that of DPCM with crystal 1 is only 35%. The above experimental results show that the crystal having a small absorption coefficients is suitable for the asymmetrical-bridge DPCM, but the crystal having a large absorption is suitable for the symmetrical-bridge DPCM. Moreover under the optimum incident conditions of asymmetrical-bridge DPCM with crystal 2, the measured response time of the DPCM is 59 s under the incident light intensity $I = I_1 = I_2 = 2$ mW.

Figure 4.5 shows the phase-conjugate transmissivity T_{pc} versus the incident light intensity I ($I = I_1 = I_2$), in Cu:KNSBN symmetrical-bridge DPCM and asymmetrical-bridge DPCM under their optimum incident conditions. The triangles show the experimental results of DPCM with crystal 2 in asymmetrical-bridge geometry. The circles show the experimental results of DPCM with crystal 1 in symmetrical-bridge geometry. These two bridge DPCMs both have high efficiencies at low incident powers. When I is only 0.12 mW, the phase-conjugate transmissivity of the DPCM with crystal 2 reaches 30% in asymmetrical-bridge geometry. Generally, small absorption and low incident power correspond to a small photorefractive effect in the crystal. Therefore, we can deduce that a crystal having a small photorefractive effect is suitable for forming the asymmetrical-bridge DPCM. This is because the DPCM made of a crystal with a small photorefractive effect needs a long interaction length for high diffraction efficiency of four-wave mixing. In the asymmetrical-bridge

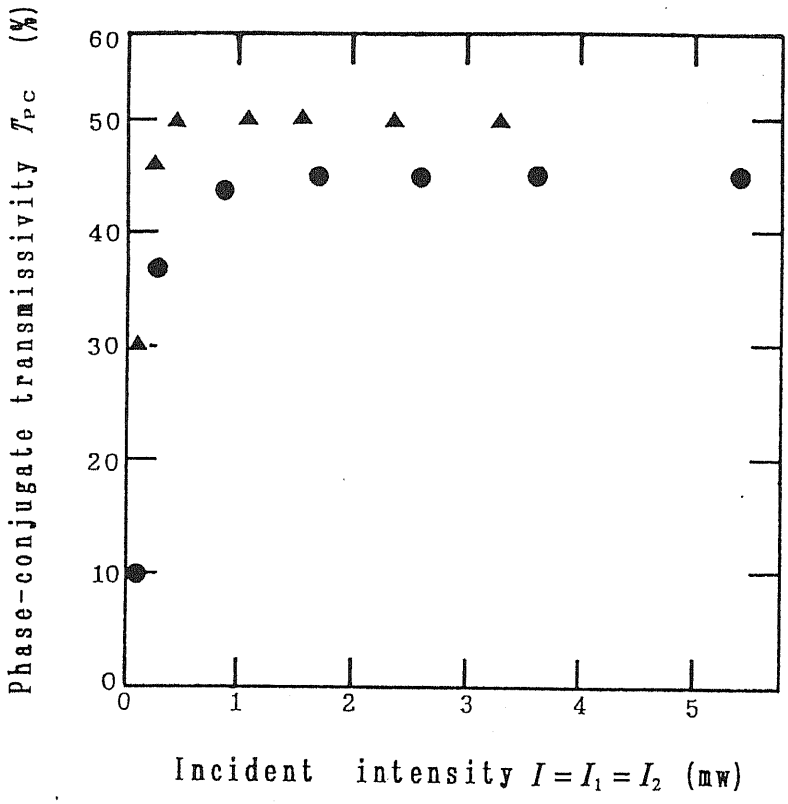

Fig. 4.5. Phase-conjugate transmissivity T_{pc} versus the incident intensity I ($I = I_1 = I_2$) for the incident light diameter d = 1.6 mm. Circles correspond to symmetrical bridge DPCM with crystal 1. Here the incident angle is $\Phi = \Phi_1 = \Phi_2 = 47°$, and the incident position is $x = x_1 = x_2 = 3.5$ mm. Triangles correspond to asymmetrical bridge DPCM with crystal 2. Here the incident angles are $\Phi_1 = 21°$, $\Phi_2 = 41°$ and the incident positions are $x_1 = 2$ mm, $x_2 = 3.3$ mm.

DPCM, the interaction length is longer than that of the symmetrical-bridge DPCM [see Figs. 4.3(a) and 4.3(b)].

4.4 Summary

In conclusion, two kinds of bridge DPCMs (symmetrical geometry and asymmetrical geometry) have been formed with Cu:KNSBN crystals having different absorption coefficients. These Cu:KNSBN bridge DPCMs have very high efficiencies. When the absorption coefficients of the crystals are different, the optimum incident geometries of forming DPCM are different. The crystal having a large absorption coefficient is suitable for forming the symmetrical-bridge DPCM, and the crystal having a small absorption coefficient is suitable for forming the asymmetrical-bridge DPCM. At very low powers, these bridge DPCMs of Cu:KNSBN crystals still have very high efficiencies.

References

1. E. J. Sharp, W. W. Clark III, M. J. Miller, G. L. Wood, B. Monson, G. J. Salamo, and R. R. Neurgaonkar, *Appl. Opt.* **29,** 743 (1990).
2. G. W. Ross and R. W. Eason, *Opt. Lett.* **15,** 571 (1993).
3. Y. Zheng, A. Sasaki, X. Gao, H. Aoyama, and J. Fukaya, *Jpn. J. Appl. Phys.* **34,** 5405 (1995).
4. X. Gao, A. Sasaki, and Y. Zheng, *Jpn. J. Appl. Phys.* **32,** L1654 (1993).
5. X. Gao, A. Sasaki, Y. Zheng, H. Aoyama, and J. Fukaya, *Opt. Rev.* **1,** 230 (1994).
6. Y. Zheng, A. Sasaki, and X. Gao, *Nonlinear Opt.* **8,** 115 (1994).
7. X. Yue, X. Lu, Y. Song, Z. Shao, D. Sun, Q. Jiang, and H. Chen, *Appl. Phys.* **B 53,** 319 (1991).
8. G. Hussain, S. W. James, and R. W. Eason, *J. Opt. Soc. Am.* B **7,** 2294 (1990).

Chapter 5

Multiple Phase-Conjugate Mirror (PCM) and Orthoscopic Projection of a Three-Dimensional (3D) Object in a Cu:KNSBN Crystal

A new type of multiple phase-conjugate mirror consisting of a self-pumped phase-conjugate mirror and a bridge double phase-conjugate mirror is presented in a Cu:KNSBN crystal, which performs two phase-conjugate operations on the incident light wave. A phase-conjugate reflectivity as high as 105% with a high stability is observed. A good fidelity of phase-conjugate image is obtained. The real-time orthoscopic three-dimensional image projection using the multiple phase-conjugate mirror is also demonstrated.

5.1 Introduction

The phase-conjugate mirrors (PCMs) have attracted special interest for a number of applications.[1-8] In photorefractive crystals, different PCMs have been reported, as described in chapter 2 and chapter 3. The use of a PCM to project

images was first reported by Levenson in 1980.[9] However, when projecting three-dimensional (3D) images, PCMs bring inconvenient viewing, because PCMs produce real pseudoscopic images with their perspective inversion. The real-time orthoscopic 3D image projection using the feedback phase-conjugate setup was realized in 1991.[9] However, the phase-conjugate reflectivity of the feedback phase-conjugate setup is not high in performing 3D image projection. This system is also unstable.[9,10]

In this chapter, a new type of multiple PCM in a Cu:KNSBN crystal is presented, which consists of a SPPCM and a bridge DPCM.[11] The multiple PCM performs two phase-conjugate operations on the incident light wave. The performance of the multiple PCM is investigated. The fidelity of the phase-conjugate image and the real-time orthoscopic projection of a 3D object are also demonstrated by use of the multiple PCM.

5.2 Two Phase-Conjugate Operations on an Input Light Wave

As described in chapter 1, optical phase conjugation is a technique that can precisely reverse both the direction of propagation and the overall phase factor for an input light wave. When an electromagnetic wave described by Eq. (1.1) is incident on a PCM, its phase-conjugate wave is given by Eq. (1.2). We can see that the incident wave and its phase-conjugate wave have exactly the same wave front at any point in space. However, the motion of these two sets of wave fronts is in opposite direction. For the projection of 3D object scenes, this means that the relation between the front and back positions in the propagation direction is inverted in the phase-conjugate images of projected 3D object, and also the left and right positions

are flipped in the cross section of the propagation direction compared with the incident images of the 3D object. Phase-conjugate reconstruction produces real pseudoscopic images with perspective inversion, which is clearly inappropriate for the projection of the 3D object. If the phase-conjugate operation is again performed for any phase-conjugate wave given by Eq. (1.2), that is, a system performs two phase-conjugate operation on the incident wave, then the secondary phase-conjugate wave is written by

$$E_{cc} = A(r)\exp\{i[\omega t - kz - \phi(r)]\}. \tag{5.1}$$

It can be seen that this is just a restoration of the incident light wave. In other words, when two phase-conjugate operations on the incident images of the 3D object are performed, the correct perspective orthoscopic projection of the 3D object can be achieved.

5.3 Formation of the Multiple PCM in a Cu:KNSBN Crystal

The formation of a Cu:KNSBN crystal SPPCM has been reported in Ref. 12. In chapter 2 and chapter 3, the high-performance DPCM and the high-efficiency bridge DPCMs have been demonstrated in Cu:KNSBN crystals. Here the new multiple PCM consisting of two PCMs (a SPPCM and a bridge DPCM) is also formed in a Cu:KNSBN crystal. In order to form two PCMs in a photorefractive crystal, the incident geometry should be well arranged. The experimental schematic of the multiple PCM is shown in Fig. 5.1. An extraordinary-polarized light beam 1 (with light intensity I_1) from an argon laser at λ = 514.5 nm is incident upon *a* face of the Cu:KNSBN crystal (6 mm × 6 mm × 6 mm) with incident angle θ. A SPPCM is

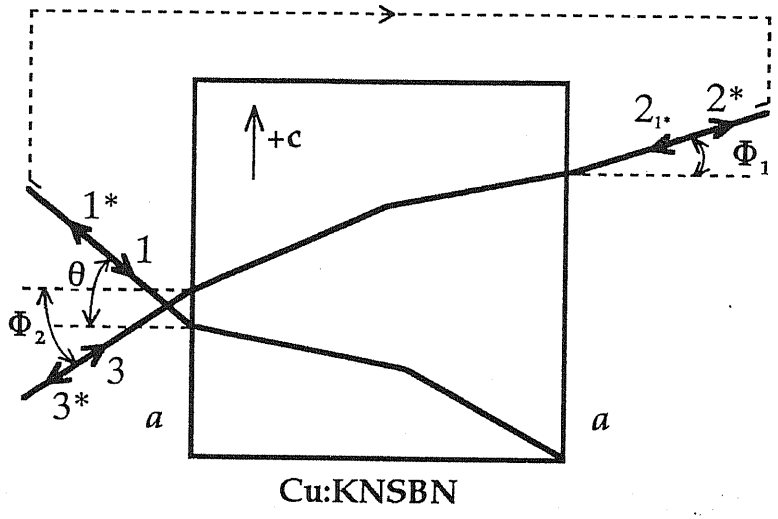

Fig. 5.1. Schematic of a Cu:KNSBN crystal multiple PCM. Incident beams 1 and 2_{1^*}, and beams 1 and 3 are mutually incoherent. θ, Φ_1, and Φ_2 are incident angles.

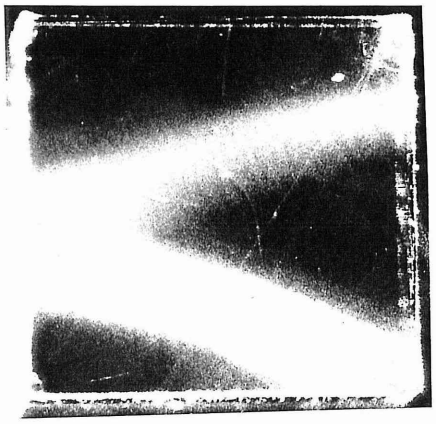

Fig. 5.2. Photograph of the formed Cu:KNSBN crystal multiple PCM.

formed. Phase-conjugate beam 1* (with light intensity I_{1pc}) of incident beam 1 is generated by the SPPCM. According to the description of Ref. 12, to obtain stable efficient SPPCM, we selected properly incident angle θ (θ = 40°). The incident light beam diameter d is 2 mm. The observed phase-conjugate light output of the SPPCM is stable. Here, the incident light intensity is 22 mW. The measured phase-conjugate reflectivity R_{1pc} ($R_{1pc} = I_{1pc}/I_1$) of the SPPCM is 46%. Further, the phase-conjugate light beam generated by the SPPCM is fed back to the other a face of the Cu:KNSBN crystal as secondary incident light beam 2_{1*} (with light intensity $I_{2(1pc)}$). The incident angle of light beam 2_{1*} is Φ_1. Meanwhile, the other extraordinary-polarized light beam 3 (with light intensity I_3) is incident upon a face of the Cu:KNSBN crystal at angle Φ_2 (see Fig. 5.1). A bridge DPCM of the Cu:KNSBN crystal is formed. The path differences of incident light beams 2_{1*} and 3, and 1 and 3 are 60 cm and 20 cm, respectively, which are much longer than the coherence length (5 cm) of the argon laser. Therefore, beam 2_{1*} and 3, and 1 and 3 are mutually incoherent. Phase-conjugate light beam 2* (with light intensity I_{2pc}) of feedback phase-conjugate light beam 2_{1*} is generated by the bridge DPCM. In the experiment, Incident angles Φ_1 and Φ_2 are 21° and 41° respectively, which correspond to the optimum incident angles of the bridge DPCM described in chapter 4. Thus, a new type of multiple PCM is formed, which performs two phase-conjugate operations on the signal input with the two PCMs (the SPPCM and the bridge DPCM) in a single Cu:KNSBN crystal. A photograph of the multiple PCM is shown in Fig. 5.2.

5.4 Performance of the Multiple PCM

Figure 5.3 shows the final phase-conjugate reflectivity R_{2pc} ($R_{2pc} = I_{2pc}/I_{2(1pc)}$) of the multiple PCM versus the ratio q ($q = I_3/I_{2(1pc)}$). When the ratio q = 4.0, a phase-

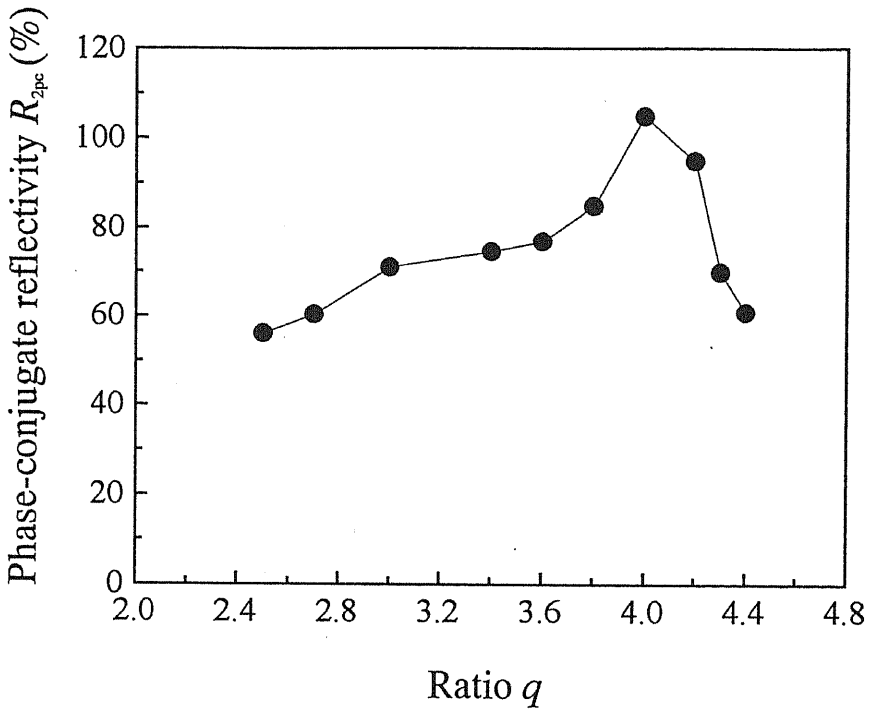

Fig. 5.3. Phase-conjugate reflectivity R_{2pc} ($R_{2pc} = I_{2pc}/I_{2(1pc)}$) of the multiple PCM versus the ratio q ($q = I_3/I_{2(1pc)}$). Here the incident angle $\theta = 40°$ in the SPPCM, and the incident angles $\Phi_1 = 21°$ and $\Phi_2 = 41°$ in the bridge DPCM.

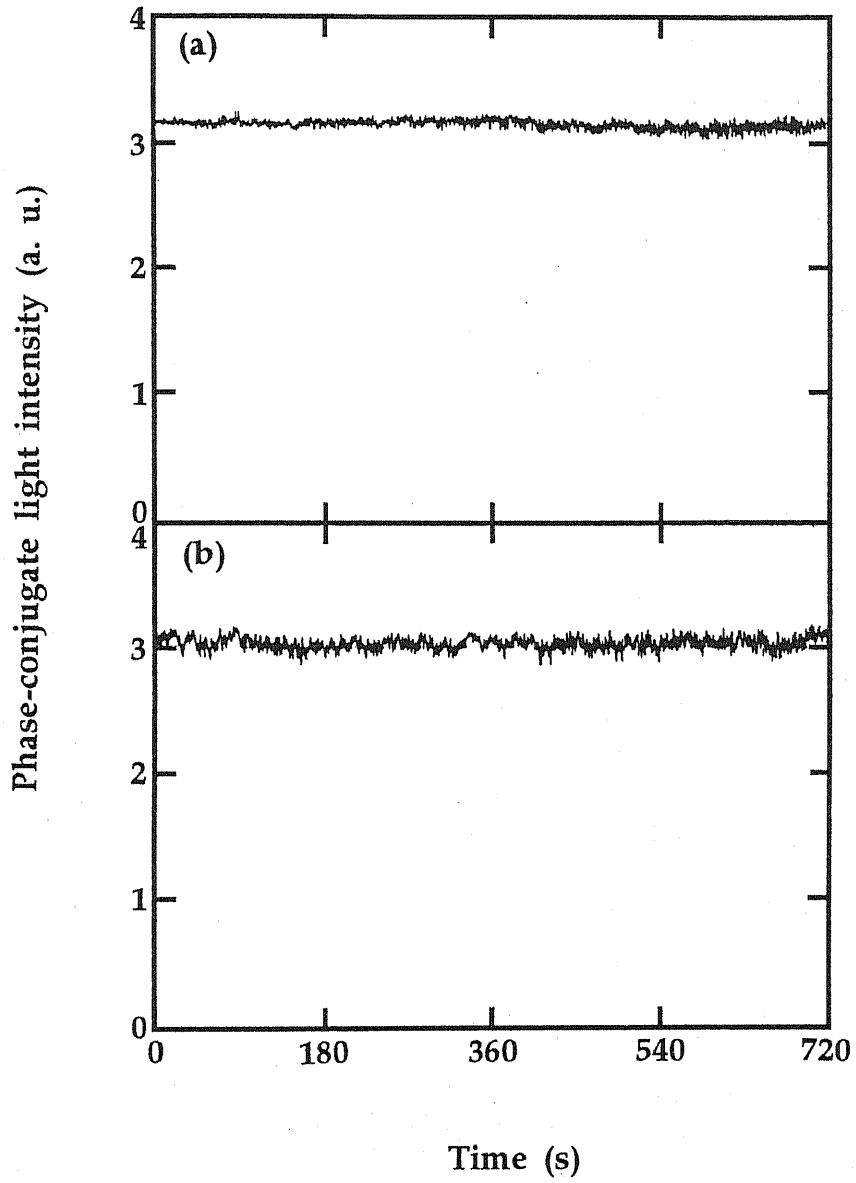

Fig. 5.4. Stability observations of recorded phase-conjugate light intensities I_{1pc} and I_{2pc} simultaneously. (a) Phase-conjugate light intensity I_{1pc} generated by the SPPCM. (b) Final phase-conjugate light intensity I_{2pc} generated by the bridge DPCM.

conjugate reflectivity as high as 105% was observed. This high value means that the Cu:KNSBN multiple PCM has good prospects for practical applications. In the multiple PCM, two large interaction regions are generated in the SPPCM and the DPCM, respectively. The large coupling constants and the large interaction regions result in high diffraction efficiencies of four-wave mixing, which has been described in chapter 3. Therefore, a high efficiency was achieved in the multiple PCM.

We also observed the stabilities of phase-conjugate light intensities I_{1pc} and I_{2pc} simultaneously, as shown in Figs. 5.4(a) and 5.4(b). The relative stabilities are about 92% and 90% respectively, which are very high values. Both phase-conjugate light intensities I_{1pc} and I_{2pc} are very stable. The multiple PCM is more stable than the feedback phase-conjugate setup described in Ref. 9. This is because the interaction regions of the two PCMs constituting the multiple PCM are separate. There is no interference between them. The stable SPPCM and the stable bridge DPCM can been formed in the Cu:KNSBN crystal, respectively. Moreover, inside the crystal, the fanning and the disturbance of the fanning to the gratings of the two PCMs are small because of their high efficiencies. Thus, a stable phase-conjugate light output of the multiple PCM is produced.

5.5 Spatial Fidelity of the Multiple PCM and Real-Time Orthoscopic 3D Image Projection

In PCMs, the spatial resolution of the phase-conjugate image is used to examine the spatial fidelity of the PCMs. Here we observed the spatial fidelity of the multiple PCM, using the experimental arrangement shown in Fig. 5.5. The incident beam diameter was expanded to 12 mm by a pair of lenses (L_1 and L_2). A standard USAF resolution test card was inserted in position D1 of the incident pass. After passing

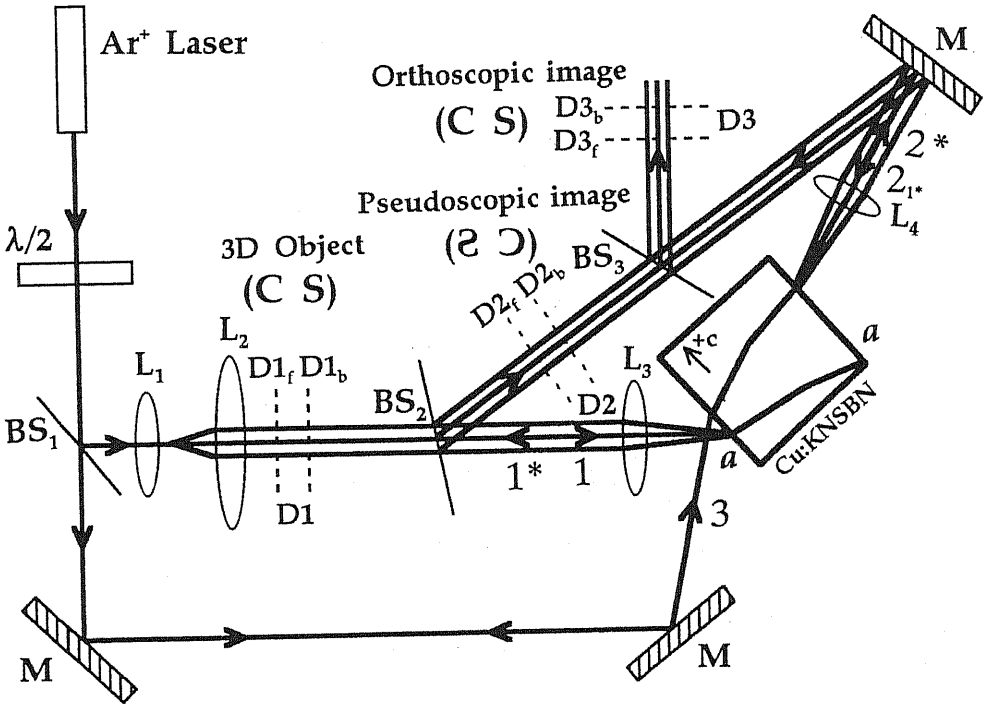

Fig. 5.5. Experimental arrangement for observing phase-conjugate images of a multiple PCM. λ/2, half-wave plate; BS's, beam splitters; L's, lenses; M's, mirrors.

through the beam splitter BS_2, the image-bearing beam was focused on *a* face of the Cu:KNSBN crystal by a lens L_3 (focal length f = 95 mm). The phase-conjugate image generated by the SPPCM was also fed back to the Cu:KNSBN crystal as secondary incident light beam 2_{1*}. Lens L_4 (focal length f = 45 mm) focused phase-conjugate light beam 2_{1*} onto the other *a* face of the crystal, and all other incident conditions are the same as shown Fig. 5.1. For the image-bearing beam, two phase-conjugate operations were performed. Figure 5.6 shows the final image generated by the multiple PCM in position D3. The resolution of the phase-conjugate image is about 22.6 line pairs/mm. This shows that the multiple PCM has a good spatial fidelity of the phase conjugation.

It is known that PCMs produce real pseudoscopic images of 3D object with their perspective inversion. Here we explored the real-time orthoscopic images projection of a 3D object, by utilizing the high-performance multiple PCM described above. In the experimental arrangement of Fig. 5.5, we removed the standard USAF resolution test card and inserted a 3D transmissive object in position D1. The 3D object is composed of two images ("C" and "S") positioned at 3 cm apart along the incident pass (the image "C" is placed at front position $D1_f$ and the image "S" is placed at back position $D1_b$), and all other experimental conditions are still same as those of Fig. 5.1. The phase-conjugate pseudoscopic images of the 3D object produced by the SPPCM with a reflectivity R_{1pc} of 42% are shown in Figs. 5.7(a) and 5.7(b), which are taken in positions $D2_f$ and $D2_b$ with 3 cm apart, respectively. The distance (3 cm) is just equal to the distance between the two images constituting the 3D object. Figure 5.7(a) shows that the projection of the image "S" placed at position $D1_b$ is clear, however the projection of the image "C" placed at position $D1_f$ is not clear. Figure 5.7(b) shows the opposite result. This means that the relation between the front and back positions of the projection images of the 3D object

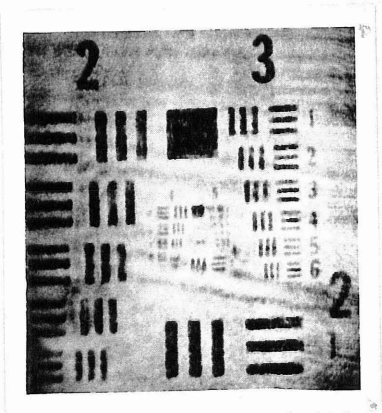

Fig. 5.6. Phase-conjugate image of the USAF resolution test card in position D3 by the multiple PCM.

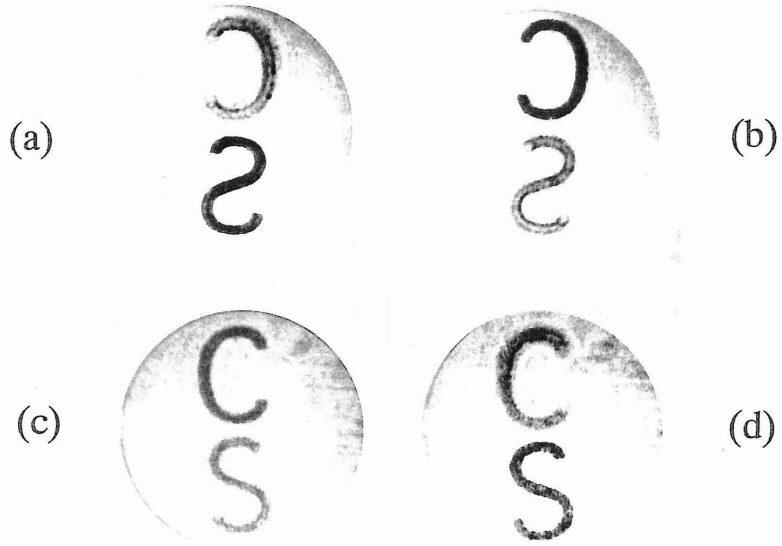

Fig. 5.7. Phase-conjugate images of the 3D object. (a), (b) Phase-conjugate pseudoscopic images of the 3D object, which are taken in positions $D2_f$ and $D2_b$, respectively. (c), (d) Phase-conjugate orthoscopic images of the 3D object, which are taken in positions $D3_f$ and $D3_b$, respectively.

produced by the SPPCM is reversed in the propagation direction compared with the incident images of the 3D object. Moreover, the relation between the left and right positions is also reversed in the cross section of the propagation direction compared with the incident images of the 3D object. This is inconvenient for viewing. When the phase-conjugate operation is again performed for the phase-conjugate pseudoscopic images [Figs. 5.7(a) and 5.7(b)] by the bridge DPCM, the real-time orthoscopic images of the 3D object are produced by the multiple PCM. The final phase-conjugate images of the projected 3D object by the multiple PCM with a reflectivity R_{2pc} as high as 102% are shown in Figs. 5.7(c) and 5.7(d). They are respectively taken in positions $D3_f$ and $D3_b$, which are also 3 cm apart. We can see that the front and back positions of the 3D object are reversed and the left and right positions are flipped in comparison with each other results [Figs. 5.7(a) and 5.7(b)] produced by the SPPCM. The real-time orthoscopic images of the 3D object are achieved, which is satisfactory for viewing. This is just as described in the second section. Thus, the correct perspective orthoscopic image projection of the 3D object is produced by the high-performance multiple PCM.

5.6 Summary

A new type of multiple phase-conjugate mirror consisting of a SPPCM and a bridge DPCM has been demonstrated, which performs two phase-conjugate operations on the incident signal in a Cu:KNSBN crystal. The stable phase-conjugate light output has been produced by taking the suitable incident geometry (a SPPCM and a bridge DPCM) with the optimum incident conditions. The multiple PCM has a very high efficiency and good fidelity. Using the high-performance multiple PCM, the real-time orthoscopic projection of a 3D object has been achieved .

References

1. J. Shamir, H. J. Caulfield, and B. M. Hendrickson, *Appl. Opt.* **27,** 2912 (1988).
2. B. Fischer, S. Sternklar, and S. Weiss, *IEEE J. Quantum Electron.* **25,** 550 (1989).
3. S. Weiss, M. Segev, S. Sternklar, and B. Fischer, *Appl. Opt.* **27,** 3422 (1988).
4. Q. C. He, J. Shamir, and J. G. Duthie, *Appl. Opt.* **28,** 306 (1989).
5. M. P. Schamschula and H. J. Caulfield, *Opt. Lett.* **16,** 1421 (1991).
6. A. Chiou, P. Yeh, C. Yang, and C. Gu, *Opt. Lett.* **20,** 1125 (1995).
7. R. J. Anderson, E. J. Sharp, G. L. Wood, and G. J. Salamo, *Appl. Opt.* **35,** 854 (1996).
8. J. M. Yarrison-Rice, E. J. Sharp, G. L. Wood, and R. R. Neurgaonkar, *Appl. Opt.* **35,** 1904 (1996).
9. N. A. Vainos and M. C. Gower, *J. Opt. Soc. Am.* B **8,** 2355 (1991).
10. M. Zhao and I. Yamaguchi, *Opt. Commun.* **112,** 163 (1994).
11. Y. Zheng, A. Sasaki, and X. Gao, *Opt. Commun.* **136,** 437 (1997).
12. X. Gao, A. Sasaki, and Y. Zheng, *Jpn. J. Appl. Phys.* **33,** 5565 (1994).

Chapter 6

All-Optical Routing Switching Dynamic Interconnection with Multiple DPCMs

An all-optical switching dynamic interconnection and an all-optical routing switching dynamic interconnection are demonstrated using the arrangements of the multiple double phase-conjugate mirrors in a photorefractive Cu:KNSBN crystal. The ON and OFF states of dynamic interconnection between the two light beams are dominated by a control beam. The dynamic interconnections of the multiple light beams are also optically switched via the incidence of different control beams.

6.1 Introduction

Interconnection devices are the basic devices in optical communication, optical computing, and optical information processing, and have attracted great attention. For critical interconnections, the alignment is very difficult because of influence of vibration, thermal drift, and other environmental factors. Specially, in waveguide optics field, the interconnections (for example waveguide-to-waveguide and fiber-to-

fiber) have been a very trouble problem which is in urgent need to be overcame for practical applications. The dynamic interconnection can compensate for vibrational, thermal, and other environmental fluctuations. In other words, the dynamic interconnection is the ideal device for these applications because of its self-adaptive and fault-tolerant properties. Optical conjugation is the most promising means of realizing the dynamic interconnection. Weiss and co-workers proposed the photorefractive dynamic optical point-to-point interconnections.[1,2] Schamschula *et al.* presented the adaptive interconnections for the message-bearing light irradiated onto the detector.[3] Recently, Chiou *et al.* reported the photorefractive spatial mode converter for multimode-to-single-mode fiber-optic coupling.[4] In these optical interconnections the double phase-conjugate mirrors (DPCMs) of the photorefractive crystals were used. The photorefractive crystals excel in providing efficient interaction of light beams even in very low power (milliwatt order). In the DPCMs the two input beam need not be mutually coherent and can be derived from separate laser.[5,6] In these interconnections, the critical optics system of collimating and focusing beams is not required, because of the generation of phase-conjugate wave. The dynamic interconnections based on the DPCMs are bidirectional, self-adaptive, fault-tolerant and efficient. However, the switching and routing switching dynamic interconnections have not been realized yet.

In this chapter, we present an all-optical switching dynamic interconnection and an all-optical routing switching dynamic interconnection, which consist of multiple DPCMs in a Cu:KNSBN crystal and a partial reflection mirror.[7] First, we describe the performance of the switching dynamic-optical interconnection between two light beams with the two DPCMs in the Cu:KNSBN crystal. Then 1 × 2 all-optical routing switching dynamic interconnection is presented with the multiple DPCMs in the crystal.

6.2 All-Optical Switching Dynamic Interconnection in a Cu:KNSBN Crystal

Double phase-conjugate mirror is four-wave mixing device, which was first reported by Weiss and co-workers in a $BaTiO_3$ crystal.[6,8] Using a Cu:KNSBN crystal, a highly efficient modified-bridge double phase-conjugate mirror[9] has been formed as described in chapter 3. The DPCM is formed from the transmission grating of four-wave mixing. As described in chapter 3, in the DPCM the high diffraction efficiency of four-wave mixing and the low light losses, including absorption and scattering loss inside the crystal, and specular reflection loss on the surfaces of the crystal, result in a very high phase-conjugate transmissivity under the Brewster angle incidence.

Here we employ this geometry to form two DPCMs in a Cu:KNSBN crystal (6 mm × 6 mm × 6 mm). We propose the arrangement of the switching dynamic interconnection using the two DPCMs (DPCM1 and DPCM2) and a partial reflection mirror M, as shown in Fig. 6.1. In our experiments the light source is an argon-ion laser at λ = 514.5 nm. All light beams are extraordinary polarized and mutually incoherent. The beam diameters are 1.6 mm. Beams 1 and 2, with intensities I_1 and I_2, are two interconnected light beams. Beam 1_i, with intensity I_{1i}, is the control beam of the dynamic optical interconnection. Beam 1_{in}, with intensity I_{1in}, is the transmission beam of the control beam 1_i through the partial reflection mirror. Beams 1 and 1_{in} are arranged under the same geometric conditions as described in chapter 3, where DPCM1 can be efficiently formed. Under the incidence of beams 1 and 2, when control beam 1_i is input, that is, beam 1_{in} is incident on the crystal, DPCM1 is formed. Simultaneously, the resulting phase-conjugate beam 1_{in}* of beam 1_{in} is reflected by the partial reflection mirror M. The reflected beam 1_r of beam 1_{in}*

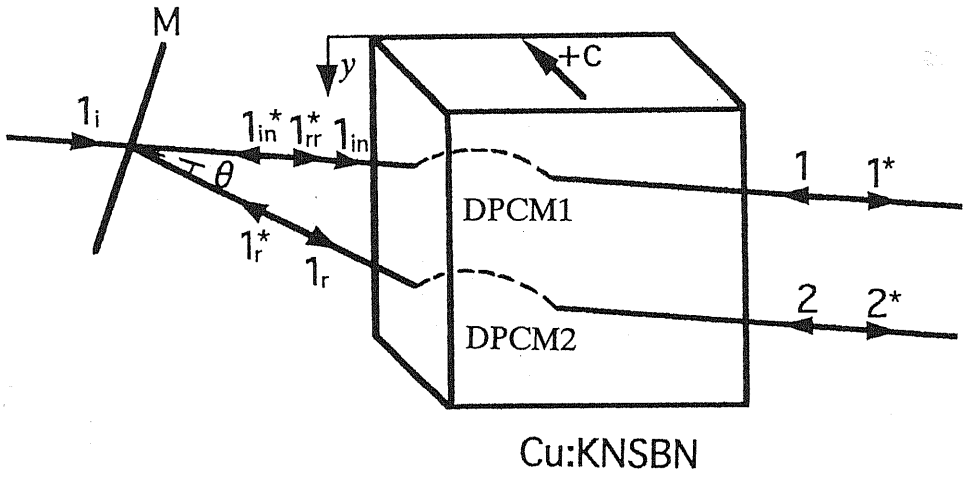

Fig. 6.1. Schematic of the switching dynamic interconnection by using two DPCMs in a Cu:KNSBN crystal, and a partial reflection mirror M.

is in the direction (at the reflection angle θ) that forms DPCM2 with beam 2. When DPCM2 is formed, the reflected beam 1_r, with intensity I_{1r}, is diffracted by the transmission grating of DPCM2 to form phase-conjugate beam 2* (intensity I_{2*}) of beam 2. Thus, by diffraction due to DPCM1, the reflection from the partial reflection mirror, and the diffraction due to DPCM2, the light of beam 1 is transformed into the phase-conjugate beam 2* of beam 2, which dynamically retraces beam 2. Meanwhile, by diffraction due to DPCM2, the reflection from the partial reflection mirror, and the diffraction due to DPCM1, the light of beam 2 is transformed into a part of phase-conjugate beam 1* (intensity I_{1*}) of beam 1, which dynamically retraces beam 1. Thus beams 1 and 2 are bidirectionally interconnected. The interconnecting efficiency is

$$\eta = T_1 R T_2, \tag{6.1}$$

where T_1 and T_2 are the phase-conjugate transmissivities of DPCM1 and DPCM2. According to the description in chapter 3, the transmissivities of DPCMs are given by

$$T_1 = \frac{I_{1*}}{I_{\text{in}}} \approx T_1' = \frac{I_{1\text{in}*}}{I_1}, \tag{6.2}$$

and

$$T_2 = \frac{I_{2*}}{I_{1\text{r}}} \approx T_2' = \frac{I_{1\text{r}*}}{I_2}, \tag{6.3}$$

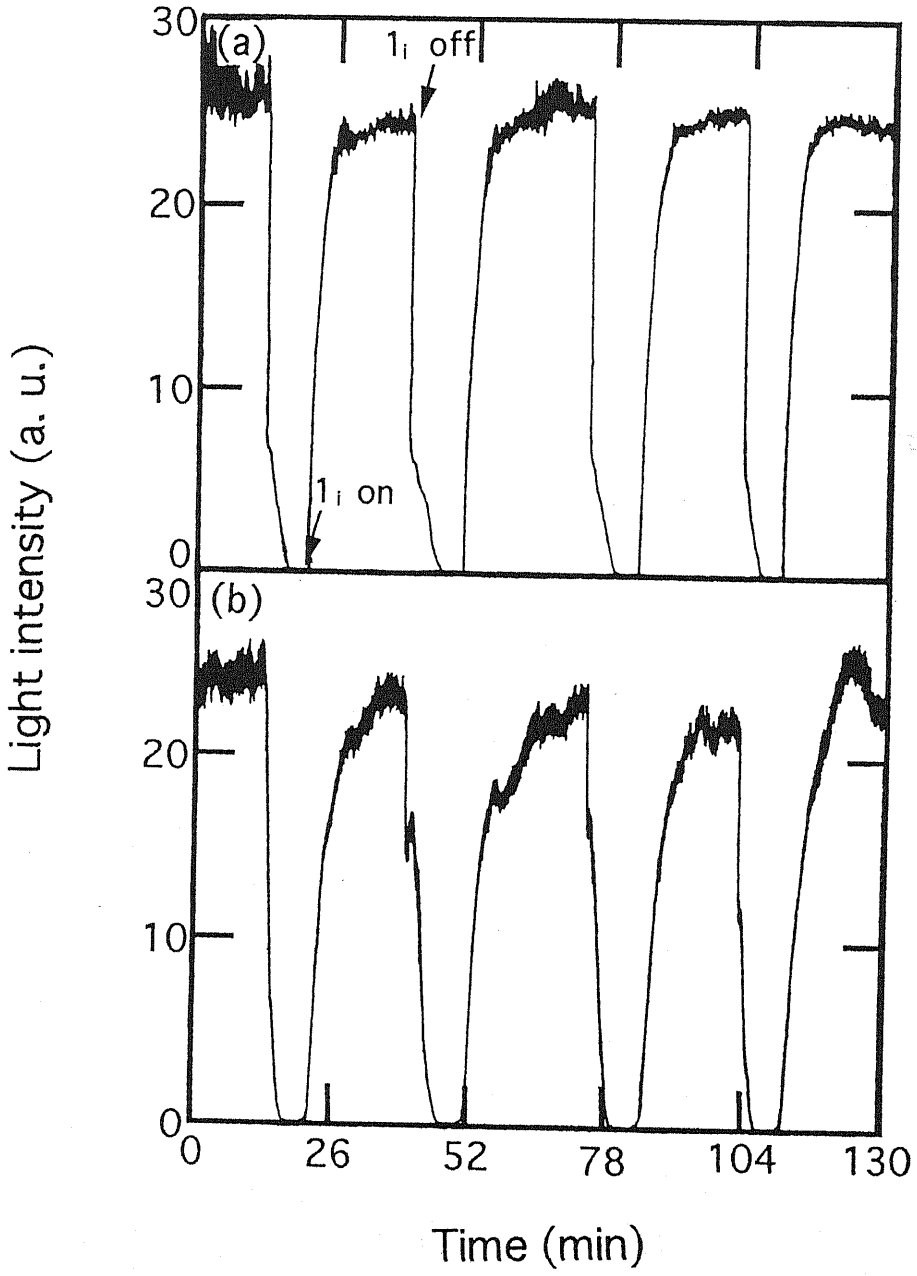

Fig. 6.2. Experimental results of the switching dynamic optical interconnection for the incidence and shut of the control beam. (a) The variation of beam 1*. (b) The variation of beam 2*.

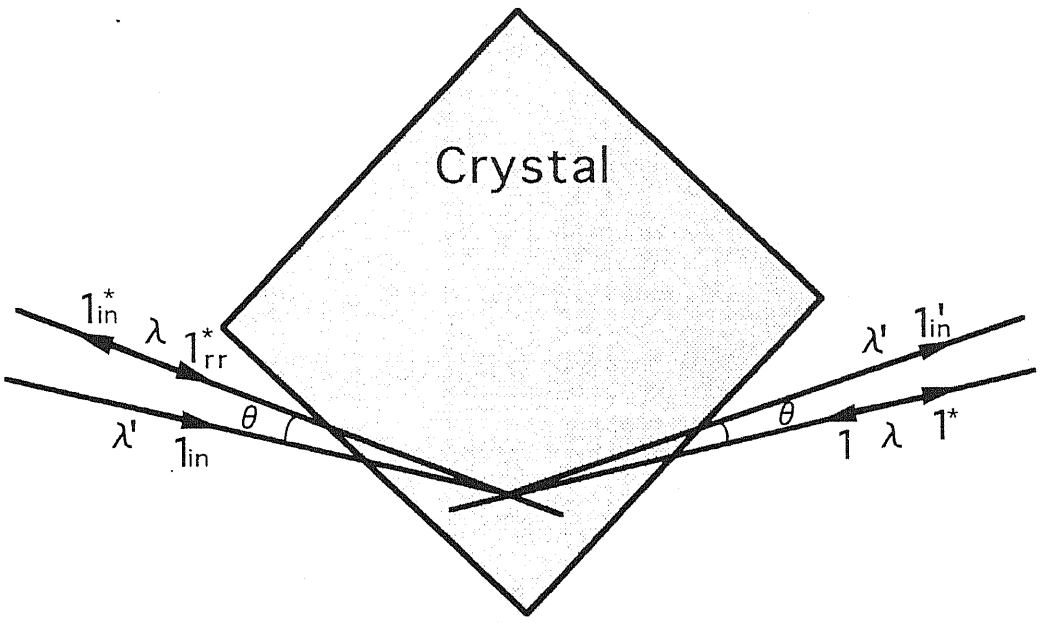

Fig. 6.3. Schematic of the double-color pumped phase-conjugate mirror with two incident beams 1 and 1_{in} of different wavelengths λ and λ'. Beams 1_{in}* and 1_{in}' are the generated phase-conjugate beams, respectively. θ is the shift angle between the incident beam and the generated phase-conjugate beam.

R is the reflectivity of the partial reflection mirror M. It can be seen that the interconnecting efficiency is directly proportional to the phase-conjugate transmissivities of the DPCMs and the reflectivity of the partial reflection mirror M. However, if the reflectivity of the partial reflection mirror M is too high, the loss of the control light is too large. Here we use a partial reflection mirror with reflectivity R = 50%. In this experiment the powers of beams 1_i, 1 and 2 are I_{1i} = 5 mW, I_1 = 4.1 mW and I_2 = 2.8 mW, respectively. The reflection angle θ is about 0.8°. The distance between the crystal and the mirror M is 13 cm. The measured phase-conjugate transmissivities of DPCM1 and DPCM2 are about 68% and 40%, respectively. The observed interconnecting efficiency is about 14%. When control beam 1_i is shut off, the DPCMs cannot be formed continuously, because the only the phase-conjugate light beam 1_{rr}* cannot support the formation of DPCM1. Thus, the interconnection enters the OFF state. Figure 6.2 shows the experimental result for the switching dynamic interconnection. When control beam 1_i is switched on, that is, beam 1_{in} (I_{1in} = 2.5 mW) is incident on the crystal, beams 1* and 2* are produced, and dynamically retrace beams 1 and 2, after the DPCMs are formed. When control beam 1_i is switched off, the interconnection enters the OFF state after the decay time of the DPCMs. This experimental result shows the achievement of an all-optical switching dynamic interconnection for the ON-OFF transition. The ON-OFF states of the dynamic interconnection are dominated by the control beam with a very low power compared with other all-optical switching devices. In the experiment, some light of beam 1* is transformed from control beam 1_i. If the wavelength of the light of the control beam is shifted (several nanometres), in beam 1*, light beam 1_{in}' transformed from control beam 1_i can produce an angle shift beyond the path of beam 1,[1,2] as shown in Fig. 6.3, or be cut using a cut filter, when the light of the control beam must be prevented from entering the pass of beam 1*.

6.3 All-Optical Routing Switching Dynamic Interconnection

Based on the above principle and experiment result, we can expect to form an all-optical routing switching dynamic interconnection. In the switching interconnection, when the control beam of a different direction (y-direction) is introduced, the generated phase-conjugate beam is reflected by the mirror M toward a different direction and connects with a different light beam. Figure 6.4 shows the experimental arrangement of 1 × 2 routing switching dynamic interconnection. The incident positions of two beams 1_{in} (I_{1in} = 9 mW) and 2_{in} (I_{2in} = 14.9 mW) (the powers of control beams 1_i and 2_i are 18 mW and 29.8 mW) are arranged at the same point on the crystal, where DPCM1 can be formed with beam 1. We perform the routing switching dynamic optical interconnections of beam 1 (I_1 = 20 mW) to beams 2 (I_2 = 8.6 mW) and 3 (I_3 = 9.4 mW). When DPCM1 is formed with control beam 1_i, the resulting phase-conjugate beam 1_{in}* is reflected by mirror M (reflection angle θ_1 = 0.4°) to form DPCM2 with beam 2. Thus, as described above paragraph, beams 1 and 2 are bidirectionally interconnected. When control beam 2_i is introduced after turning off control beam 1_i, the resulting phase-conjugate beam 2_{in}* is reflected toward the crystal by mirror M and forms the DPCM3 with beam 3 (reflection angle θ_2 = 0.9°). In the same manner as described above, the interconnection between beams 1 and 3 is completed. Thus, all-optical routing switching dynamic interconnections of multiple beams are achieved. The experimental results are shown in Fig. 6.5. The dynamic interconnections of the multiple light beams are switched by inputting different control beams, 1_i and 2_i. The interconnecting efficiencies of about 15% and 24% between beams 1 to 2 and 1 to 3, respectively, were observed. This is the first successful achievement of the routing switching dynamic interconnections to our knowledge. The routing switching dynamic interconnection

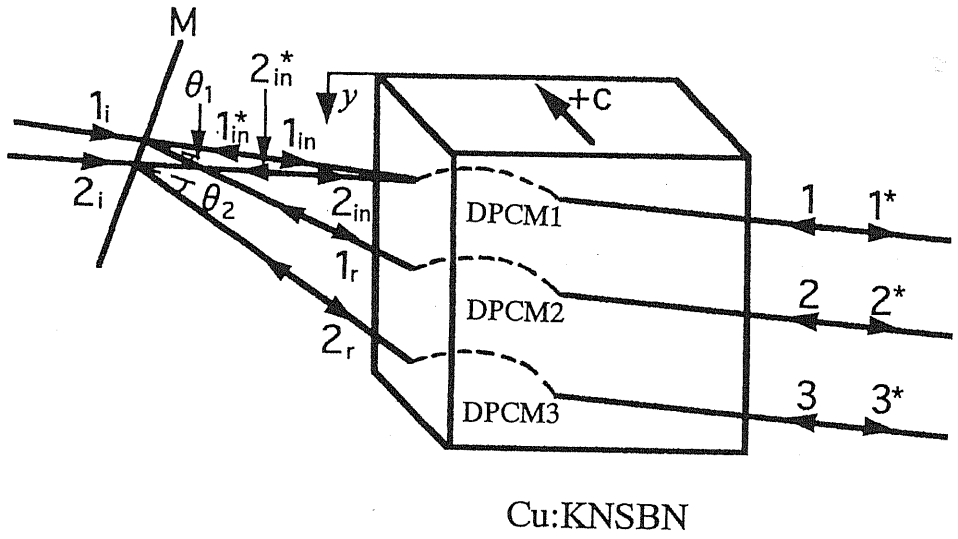

Fig. 6.4. Schematic of the experimental arrangement of 1 × 2 routing switching dynamic interconnection.

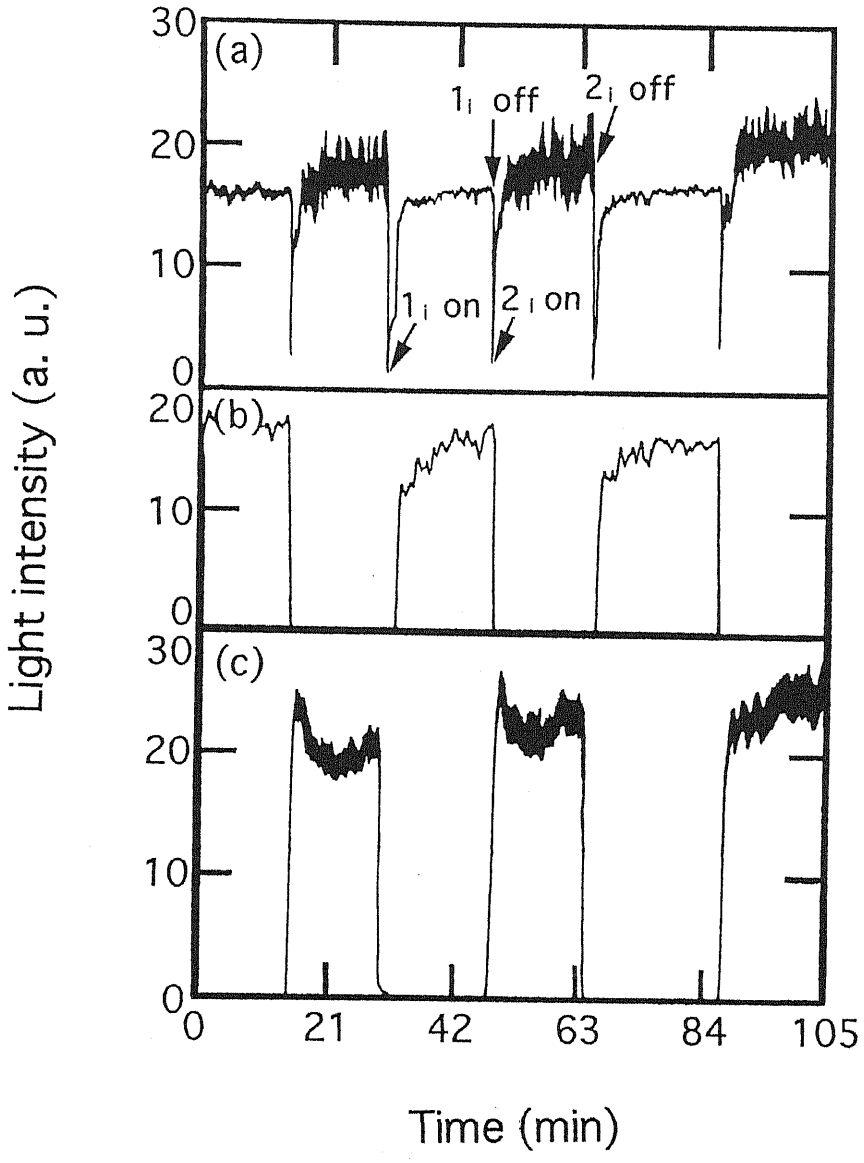

Fig. 6.5. Observation of the dynamic interconnections between beams 1 to 2 and 1 to 3 by alternately inputting control beams 1_i and 2_i. (a) The variation of beam 1*. (b) The variation of beam 2*. (c) The variation of beam 3*.

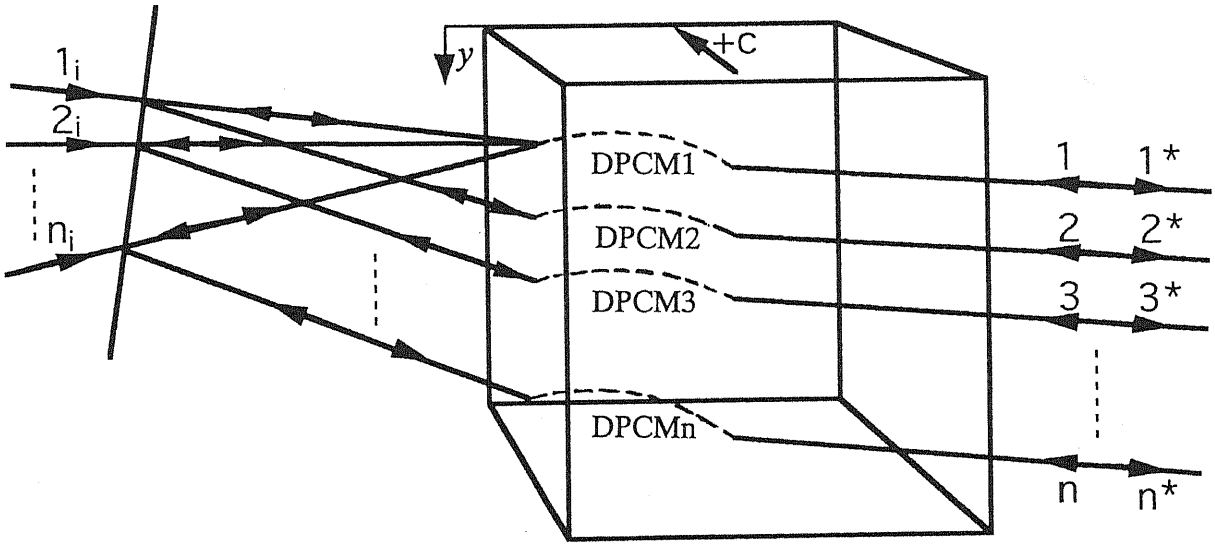

Fig. 6.6. Schematic of 1 × n routing switching dynamic interconnection with more DPCMs.

device can be used for waveguide-to-waveguide, fiber-to-fiber, light source-to-waveguide, message-bearing beam-to-detector, and laser-to-laser connections.

In our experiment, the switching time of the dynamic interconnection is decided by the formation and decay time of the DPCMs. On comparing the experimental results of the switching dynamic interconnection and the routing switching dynamic interconnection (Fig. 6.2 and Fig. 6.5), we can see that the response time in Fig. 6.5 is faster than that in Fig. 6.2. We believe that there are two aspects contributing to the fast response of the routing switching dynamic interconnection. First, the incident power is higher in Fig. 6.5. Second, the two sets of overlapped gratings of beams 1_{in} to 1 and 2_{in} to 1 enhance the response speeds to each other in alternate formation and decay of the DPCMs. In another aspect, if the light densities of the incident beams are sufficiently increased, or a photorefractive crystal (such as $BaTiO_3$) with fast response is used, the response time of the dynamic interconnections of the multiple light beams can be as fast as the order of second. Otherwise, when cylindrical lenses are used to decrease the incident beam diameters in the y-direction, the routing switching dynamic interconnections having more beams with more DPCMs can be formed, as shown in Fig. 6.6.

6.4 Summary

In conclusion, we have demonstrated an all-optical switching dynamic interconnection and an all-optical routing switching dynamic interconnection with multiple double phase-conjugate mirrors in a Cu:KNSBN crystal, and a partial reflection mirror. The dynamic interconnection is dominated by a control beam with a very low power (milliwatt order). The dynamic interconnections are also switched by inputting the different control beam. 1 × 2 all-optical routing switching dynamic

interconnection has been formed. The observed interconnecting efficiency is high. This is the first successful achievement of a switching dynamic interconnection and an all-optical routing switching dynamic interconnection to our knowledge.

References

1. S. Weiss, M. Segev, S. Sternklar, and B. Fischer, *Appl. Opt.* **27,** 3422 (1988).
2. B. Fischer, S. Sternklar, and S. Weiss, *IEEE J. Quantum Electron.* **25,** 550 (1989).
3. M. P. Schamschula, H. J. Caulfield, and C. M. Verber, *Opt. Lett.* **16,** 1421 (1991).
4. A. Chiou, P. Yeh, C. Yang, and C. Gu, *Opt. Lett.* **20,** 1125 (1995).
5. S. Weiss, S. Sternklar, and B. Fischer, *Opt. Lett.* **12,** 114 (1987).
6. S. Sternklar, S. Weiss. M. Segev, and B. Fischer, *Opt. Lett.* **11,** 528 (1986).
7. Y. Zheng and A. Sasaki, *Jpn. J. Appl. Phys.* **36,** L676 (1997).
8. S. Weiss, S. Sternklar, and B. Fischer, *Opt. Eng.* **26,** 432 (1987).
9. Y. Zheng, A. Sasaki, X. Gao, and H. Aoyama, *Opt. Commun.* **116,** 449 (1995).

Chapter 7

Conclusion

The stable self-pump phase-conjugate mirror (SPPCM) and the high-performance double phase-conjugate mirrors (DPCMs) in Cu:KNSBN crystals have been studied in detail. A new type of multiple phase-conjugate mirror has been formed, which has been used to achieve the real-time orthoscopic projection of a three-dimensional object. A routing switching dynamic interconnection has been also presented. In the last chapter, a summary of the thesis and some suggestions to further study are given.

7.1 Summary

In this thesis, the high-performance phase-conjugate mirrors (PCMs) and applications of PCMs have been studied. In chapter 1, an introduction on optical phase conjugation and the outline of the thesis have been given.

In chapter 2, a theory of two-wave mixing has been described, which have been used to explain the self-generated fanning effect in a SPPCM. The dynamic instability in the SPPCM has been further investigated. The dynamic instability

originating from the competition between the self-generated fanning effect and SPPCM formation has been analyzed and proved. The theory and experiment results show that the self-generated fanning effect in a photorefractive crystal can be decreased by the ordinary-polarized component of a partially extraordinary-polarized incident light beam. The dynamic instability of the SPPCM can be eliminated by restraining the self-generated fanning effect.

In order to reveal the performance of DPCM, a theory of four-wave mixing for a DPCM has been given in chapter 3. It is shown that the large coupling strength corresponds to high phase-conjugate efficiency. How to form a high-performance DPCM has been demonstrated in a Cu:KNSBN photorefractive crystal. Based on the high diffraction efficiency of four-wave mixing and the low light losses including absorption and scattering loss inside the crystal, and specular reflection loss on the surfaces of the crystal, a high-performance modified-bridge DPCM has been formed with a low incident power (milliwatt order) in a Cu:KNSBN crystal. A phase-conjugate transmissivity as high as 63% with 97% relative stability has been observed in Brewster angle incidence. The efficiency of the modifield-bridge DPCM is the highest value in the reported DPCMs to our knowledge.

In chapter 4, two kinds of bridge DPCMs with the symmetrical geometry and asymmetrical geometry have been formed in Cu:KNSBN crystals. These Cu:KNSBN bridge DPCMs have high efficiencies. For the crystals with different absorption coefficients, the optimum incident geometries of forming DPCM are different. The crystal having a large absorption coefficient is suitable for forming the symmetrical-bridge DPCM. The crystal having a small absorption coefficient is suitable for forming the asymmetrical-bridge DPCM. Even if at very low incident power, these bridge DPCMs still have high efficiencies.

In chapter 5, a new type of multiple phase-conjugate mirror consisting of two

PCMs, which performs two phase-conjugate operations on the incident light wave, has been demonstrated in a Cu:KNSBN crystal. The stable phase-conjugate light output has been produced by use of the suitable incident geometry (a SPPCM and a bridge DPCM) with the optimum incident conditions. A phase-conjugate reflectivity as high as 105% has been measured. A good fidelity of phase-conjugate image has been observed. Moreover, under two phase-conjugate operations on the image-bearing light wave, the real-time orthoscopic projection of a three-dimensional object has been achieved using the high-efficiency multiple PCM.

Another exciting application of PCM has been presented in chapter 6. An all-optical switching dynamic interconnection has been demonstrated using the arrangements of the multiple DPCMs in a Cu:KNSBN crystal, and a partial reflection mirror. The transition of the ON and OFF states for dynamic interconnection between the two light beams is dominated by a control beam with a very low power (milliwatt order). Further, an all-optical routing switching dynamic interconnection has been successfully realized. The routing dynamic interconnections are switched via the incidence of the different control beams.

7.2 Suggestions

This thesis has studied the stability of the SPPCM, the DPCMs, and some applications of the PCMs in Cu:KNSBN crystals. Many important and interesting results have been obtained. However, there are still some interesting subjects that require to be further studied.

We have successfully achieved 1 × 2 routing switching dynamic interconnection. If cylindrical lenses are used to decrease the incident beam diameters, the switching dynamic interconnections having more beams with more

DPCMs can be formed. Meanwhile the response speed can be greatly enhanced because the light density is increased. If the partial reflection mirror is directly coated onto the surface of the crystal, the device will be compact. This is a very interesting and important study subject. The routing switching dynamic interconnection device can be applied in the interconnection of waveguide-to-waveguide, fiber-to-fiber, light source-to- waveguide, and so on. In another aspect, the study of dynamic optical memory is interesting using multiple DPCMs in a photorefractive crystal. Finally, it is considered that these high-performance PCMs can be also used in many other practical applications.

Acknowledgements

I would like to express the deepest appreciation to my director, Professor Akira Sasaki, for his continued guidance, earnest encouragement and kind help. Without his persistent support this thesis would not have been possible. I am also greatly indebted to Professor Junji Ohtsubo, Professor Tomuo Yamaguchi, Professor Hiroshi Fujiyasu, and Professor Yoshinori Hatanaka for their useful discussions, valuable advice, and critical reading for this thesis. I am particularly indebted to the Japanese Monbusho for providing the Monbusho Scholarship to study in Shizuoka University.

I would like to acknowledge to Dr. Jisuke Fukaya, Mr. Futoshi Iwata, and Associate Professor Hisayuki Aoyama for their amicably helps and enjoyable discussions. I am also grateful to my colleagues in Sasaki laboratory for their various cooperations during the past three years.

Finally, I wish to express my deeply grateful to my husband, Xin Gao, for his help and encouragement to complete this thesis. My sincere thanks are also extended to my son for his love and support of time.

List of Publications by the Author

List of Papers

1. Y. Zheng and A. Sasaki, "All-optical switching dynamic interconnection with multiple mutually pumped phase conjugators," *Jpn. J. Appl. Phys.* **36,** L676 (1997).
2. Y. Zheng, A. Sasaki, and X. Gao, "Multiple phase conjugator and orthoscopic projection of three-dimensional object in a Cu:KNSBN crystal," *Opt. Commun.* **136,** 437 (1997).
3. Y. Zheng, A. Sasaki, X. Gao, H. Aoyama, and J. Fukaya, "High-efficiency bridge double phase-conjugate mirrors in Cu-doped $(K_{0.5}Na_{0.5})_{0.2}(Sr_{0.61}Ba_{0.39})_{0.9}Nb_2O_6$ crystals," *Jpn. J Appl. Phys.* **34,** 5404 (1995).
4. Y. Zheng, A. Sasaki, X. Gao, and H. Aoyama, "High-performance double phase-conjugate mirror in KNSBN:Cu crystal," *Opt. Commun.* **116,** 449 (1995).
5. Y. Zheng, A. Sasaki, X. Gao, and H. Aoyama, "Origin and elimination of dynamic instability in a self-pumped phase-conjugate mirror," *Opt. Lett.* **20,** 267 (1995).
6. Y. Zheng and A. Sasaki, "Formation and application of multiple phase-conjugate mirror in a Cu:KNSBN crystal," *Reports of Grad. School of Electron. Sci. Technol. Shizuoka University,* **18,** 65 (1997).
7. Y. Zheng, A. Sasaki, and X. Gao, "Bird-wing double phase-conjugate mirror in a KNSBN:Cu crystal," *Nonlinear Opt.* **8,** 115 (1994).
8. X. Gao, A. Sasaki, Y. Zheng, H. Aoyama, and J. Fukaya, "Phase-conjugate imaging properties in high-efficiency KNSBN:Cu double phase-conjugate mirror," *Opt. Rev.* **2,** 230 (1994).

9. X. Gao, A. Sasaki, and Y. Zheng, "Formation mechanism of self-pumped phase-conjugate mirror using a Cu-doped $(K_{0.5}Na_{0.5})_{0.2}(Sr_{0.61}Ba_{0.39})_{0.9}Nb_2O_6$ crystal," *Jpn. J. Appl. Phys.* **33,** 5565 (1994).
10. X. Gao, A. Sasaki, and Y. Zheng, H. Aoyama, and J. Fukaya, "Double phase-conjugate mirrors in KNSBN:Cu crystal," *Proc. SPIE,* **2321,** 568 (1994).
11. X. Gao, A. Sasaki, and Y. Zheng, "Incident beam condition dependence of ratio between two phase-conjugate transmissivities in double-phase-conjugate mirror," *Opt. Commun.* **106,** 258 (1994).
12. X. Gao, A. Sasaki, and Y. Zheng, "Stable high-efficiency double-phase-conjugate mirror in a Cu-doped potassium sodium strontium barium niobate crystal," *Jpn. J. Appl. Phys.* **32,** L1654 (1993).
13. X. Gao, A. Sasaki, and Y. Zheng, "Enhancement of time response of self-pumped phase-conjugate mirror in KNSBN:Cu crystal using cylindrical lenses," *Jpn. J. Appl. Phys.* **32,** 4303 (1993).

口頭発表 (全国大会、学術講演会)

1. 鄭 宇進、佐々木 彰： Cu:KNSBN 結晶における制御可能なダイナミックインタコネクト, 第 44 回応用物理学関係連合講演会 (1997 年 3 月)
2. 鄭 宇進、佐々木 彰、岩田 太、高 新： Cu:KNSBN 結晶における複合位相共役鏡の形成と 3 次元物体の正視投射, 光学連合シンポジウム福岡’96 (1996 年 9 月)
3. 田中 宏治、佐々木 彰、鄭 宇進、土井 公人、岩田 太： 高効率リング型自己励起位相共役鏡, 第 57 回応用物理学会学術講演会 (1996 年 9 月)
4. 鄭 宇進、佐々木 彰、高 新、岩田 太： フォトリフラクティブ結晶における自己発生ファニングのダイナミック不安定性, 第 43 回応用物理学関係連合講演会 (1996 年 3 月)
5. 鄭 宇進、佐々木 彰、高 新、青山 尚之、深谷 助次： Cu:KNSBN 結晶における高効率二重位相共役鏡の形成, 第 12 回強誘電体応用会議 (1995 年 5 月)
6. 鄭 宇進、佐々木 彰、高 新、青山 尚之、深谷 助次： 自己励起位相共役鏡のダイナミック不安定性の起源と消去, 第 42 回応用物理学関係連合講演会 (1995 年 3 月)
7. 円尾 健一朗、佐々木 彰、中本 充彦、鄭 宇進、青山 尚之： KNSBN:Ce による半導体レーザーを用いた位相共役光の発生, 第 42 回応用物理学関係連合講演会 (1995 年 3 月)
8. 鄭 宇進、佐々木 彰、高 新： KNSBN:Cu 結晶における高性能の位相共役鏡の形成, 光学連合シンポジウム浜松’94 (1994 年 9 月)
9. 高 新、佐々木 彰、鄭 宇進： 自己励起位相共役鏡のダイナミック不安定性の起源とコントロール, 光学連合シンポジウム浜松’94 (1994 年

9月)

10. 高　新、佐々木　彰、鄭 宇進： KNSBN:Cu 結晶における自己励起位相共役鏡の形成機構, 第11回強誘電体応用会議　(1994年5月)
11. X. Gao, A. Sasaki, Y. Zheng, H. Aoyama, and J. Fukaya: Phase-conjugate imaging properties in high-efficiency double phase-conjugate mirror, (Frontiers in information optics) ICO Topical Meeting 1994 Kyoto　(1994年4月)
12. 高　新、佐々木　彰、鄭 宇進： KNSBN:Cu 結晶を用いた高効率二重位相共役鏡形成, 第54回応用物理学会学術講演会　(1993年9月)
13. 高　新、佐々木　彰、鄭 宇進： シリンドリカルリンズを用いたKNSBN:Cu 結晶自己励起位相共役鏡の応答時間向上, 第 10 回強誘電体応用会議　(1993年5月)
14. 高　新、佐々木　彰、鄭 宇進： レーザービーム径による自己励起位相共役鏡の応答特性, 第40回応用物理学関係連合講演会　(1993年3月)